APPLICATION OF A SATELLITE BASED RAINFALL-RUNOFF MODEL FOR LARGE SCALE FLOOD SIMULATION: A CASE STUDY OF CUVELAI BASIN IN NAMIBIA

PRICILA KETAI MABANDE

April, 2011

SUPERVISORS:
Dr. Ing. T.H.M. Rientjes
Dr. B.H.P Maathuis

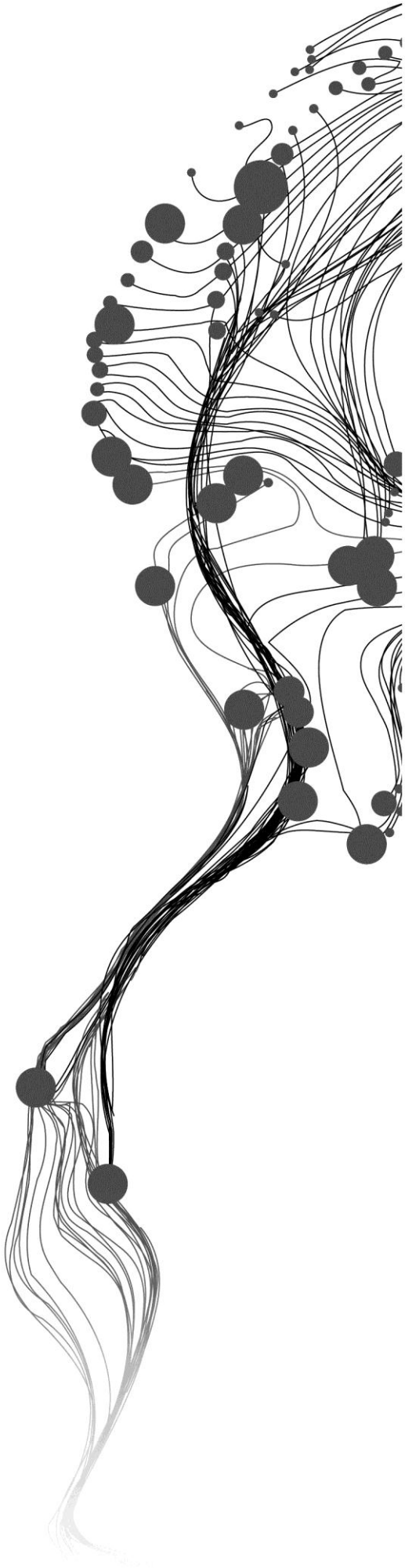

APPLICATION OF A SATELLITE BASED RAINFALL-RUNOFF MODEL FOR LARGE SCALE FLOOD SIMULATION:

A CASE STUDY OF CUVELAI BASIN IN NAMIBIA

PRICILA KETAI MABANDE
Enschede, The Netherlands, April, 2011

Thesis submitted to the Faculty of Geo-Information Science and Earth Observation of the University of Twente in partial fulfilment of the requirements for the degree of Master of Science in Geo-information Science and Earth Observation.
Specialization: Water Resources and Environmental management

SUPERVISORS:
Dr. Ing. T.H.M. Rientjes
Dr. B.H.P Maathuis

THESIS ASSESSMENT BOARD:
Dr. Ir. C.M.M. Mannaerts (Chair)
Dr. M.W. Straatsma [(External Examiner), ITC]

ABSTRACT

Distributed hydrological models are an effective tool for analysing catchment response to extreme rainfall events. However, most distributed models require extensive parameterisation and calibration, which increases model prediction uncertainty. The aim of this study is to develop a satellite based rainfall-runoff model for flood simulation in Cuvelai basin, Namibia.This study adapts the structure and format of the LISFLOOD hydrological model. LISFLOOD is a spatially distributed hydrological model that is partly physically-based. It is embedded within a PCRaster GIS environment and runs on a Python interface. The model simulates river discharges in drainage basins as a function of spatial information on soils, topography and land cover. In this study five key parameters in the model are selected for calibration and sampled using root mean squared error (RMSE) and Nash Sutcliffe coefficients. These parameters are the upperzone time constant (UZTC), lower zone time constant (LZTC), ground water percolation value (GPV), Xinanjiang parameter b (Xb) and power preferential bypass flow (PPF). Calibration of LISFLOOD was carried out by trial and error through manually adjusting the each of the parameters while visually inspecting the agreement between the observed and simulated discharges. The uncertainty of predicted discharges at the Cuvelai-basin are narrow in the peak and broad in the ascension and recession limbs. The results show that the simulation of a flood event from a short time frame of 40 days is possible , but can be improved by better calibration, possibly through replacement of single value parameters with heterogenous maps. Replacement of daily average rainfall with a higher temporal resolution such as 3 hourly rainfall can increase the model's accuracy in quantifying discharge. It is recommended that an automatic calibration procedure be used to eliminate bias introduced by manual calibration.

Key words: floods, PCRaster, LISFLOOD, hydrological model, Cuvelai basin

ACKNOWLEDGEMENTS

I would like to thank God for giving me the strength to look past many physical challenges and social obstacles and see this project to completion. It has been a long journey, with as many truimphs as there have been disappointments and frustrations.

Many thanks go to my project advisors Tom and Ben for their encouragement and many consultations. I express sincere gratitude to my colleague Max Sotomayor for paving the way with LISFLOOD and making it a little easier for me. Special thanks go to Peter Burek and Ad De Roo of JRC for their useful observations regards the input files that were critical for the successful running of the model. I also thank my colleagues Shelton and Prudence for their technical assistance with other non-model related but equally important contributions that facilitated the completion of this thesis.

The data used in this effort were acquired as part of the activities of NASA's Science Mission Directorate, and are archived and distributed by the Goddard Earth Sciences (GES) Data and Information Services Center (DISC). TRMM v6 3B42 analyses and visualizations used in this study were produced with the Giovanni online data system, which was developed and is maintained by the NASA GES DISC at the following link: http://disc.sci.gsfc.nasa.gov/additional/citing-our-data.

Many thanks to Dr. Tobias Schneiderhan and Stephanie of German Aerospace Center (DLR) who provided the flood maps used in the validation of the model. In addition I would like to thank Pauline Mufeti and the governement of Namibia for their efforts to share data on the Cuvelai catchment.

A heartfelt thank you to all staff members and lecturers from the water resources department who were not only helpful, but also friendly and encouraging. You will be missed, but not forgotten.

Last but not least, I am grateful to my family for their constant encouragement and support , especially my son, Charles Thabelang, for patiently waiting 18 months plus , for 'mommy' to finish school and come back home.

TABLE OF CONTENTS

LIST OF FIGURES

LIST OF TABLES

ABBREVIATIONS AND ACRONYMS

3B42-RT	TRMM 3B42 Real Time (experimental product)
AMSR-E	Advanced Microwave Scanning Radiometer-Earth Observing System
AMSU-B	Advanced Microwave Sounding Unit-B
CAMS	Climate Assessment and Monitoring System
CGIAR-CSI SRTM	Consultative Group on International Agricultural Research Consortium for Spatial Information
CERES	Cloud and Earth Radiant Energy Sensor
CORINE	Coordinate Information on the Environment
DEM	Digital Elevation Model
DMSP	Defense Meteorological Satellite Program
DWAF	Department of Water Affairs and Forestry [DWA till March 2005]
ENVISAT	Environmental Satellite
EGM96	Earth Gravitational Model
EUMETSAT	European Organisation for the Exploitation of Meteorological Satellites
FAO	Food and Agriculture Organisation
FOV	Field Of View
GEO	Geostationary Earth Orbit
GPROF	Goddard Profiling Algorithm
GSFC	Goddard Space Flight Center
GPCP	Global Precipitation Climatology Project
GPCC	Global Precipitation Climatological Center
GLOBCOVER	Global Land Cover
HQ-VAR	High Quality Variable Rain Rate
JAXA	National Space Development Agency of Japan
LEO	Low Earth Orbit
LIS	Lightning Imaging Sensor
LCCS	Land Cover Classification System
LSA SAF	Land Surface Analysis Satellite Application Facility
MAWF	Ministry on Agriculture, Water and Forestry [MAWRD till March 2005]
MERIS FR	Medium Resolution Imaging Spectrometer Full Resolution
NASA	National Aeronautics Space Agency
NESDIS	National Environmental Satellite Data and Information Service
NCAR	National Center for Atmospheric Research
NHS	Namibia Hydrological Services
NOAA	National Oceanic and Atmospheric Administration
NWS	Namibia Weather Services
UNDP	United Nations Development Programme
SADC-HYCOS	Southern African Development Countries Hydrological Cycle Observing System
SRTM	Shuttle Radar Topography Mission
TMI	TRMM Microwave Imager
TMPA	TRMM Multi-Satellite Precipitation Analysis
TRMM	Tropical Rainfall Measuring Mission
UNESCO	United Nations Educational Scientific and Cultural Organization
USGS	United States Geological Survey
UTM	Universal Transverse Mercator

1. INTRODUCTION

1.1. Background

In 2009 large scale floods in Cuvelai basin (Namibia) caused damage of over (USD) $500 million, (DWAF 2010). Intense and continuous rains throughout northern Namibia, southern Angola and western Zambia contributed to the flood. The floods led to the development of new hydrological conditions and drainage patterns as dried out lakes filled up (lake Liambezi) and fossil channels started to flow (Selinda river connecting to Kavango river), (NHS 2010). The floods caused emergency disaster conditions for one third of Namibia's population: 147 lives were lost, over 30 000 people displaced, agriculture and economic activities were disrupted, there was damage to infrastructure, and the government of Namibia declared a state of emergency (NHS 2010). Current climate change models anticipate higher occurrences of hydro-meteorological extremes for both droughts and floods in the near future.

1.2. Significance of the study

Lack of data constitutes the biggest challenge to hydrological studies in developing countries, thereby limiting their capacity to predict, assess and plan for the water resources within catchments (Gebremichael and Hossain 2010). The Cuvelai basin flood of 1998 which occurred in Namibia revealed that there were insufficient records of meteorological events in the past thirty years from which to infer historical flooding patterns. A post-flood investigation by SADC-HYCOS showed that there were no operational stations upstream of Namibia, in the part of Cuvelai located in Angola. The stream and rain gauges which are available are few and poorly distributed to represent the 167400km^2 size Namibia-Angola trans-boundary basin, (NHS 2010). Estimates of satellite based accumulated rainfall have to be made to better understand the spatio-temporal relationship between extreme rainfall inputs and floods. This study is an attempt to solve the problem of data scarcity for management of large and possibly trans-boundary river basins in Africa. The study aims to increase understanding of the applicability of satellite based rainfall estimation products as major inputs to rainfall-runoff models for flood simulation.

1.3. Objectives and research questions

1.3.1. General objective

The main objective of this study is to develop a satellite based rainfall-runoff model for flood simulation in Cuvelai basin in Namibia.

1.3.2. Specific objectives

- To identify satellite based rainfall estimation products that have high temporal resolution over the Cuvelai basin.

- To apply remote sensing based approaches for rainfall estimation in the Cuvelai basin.
- To identify and apply a model that allows for rainfall-runoff simulation of an extreme rain event, leading to demonstration of flood inundation in the Cuvelai basin.

1.3.3. Research questions

- Which satellite based rainfall product (s) with high temporal resolution can be used to estimate rainfall in Cuvelai basin?
- What is the effect of high rainfall events in upper Cuvelai (Angola) on downstream Cuvelai (Namibia) in space and time?
- Which model can be applied or adapted to carry out the Cuvelai basin research to simulate a flood from an extreme rain event on a large river basin?
- How can the input parameter maps and tables of LISFLOOD rainfall runoff model be adapted to accommodate the data sources and formats existing for Cuvelai basin?

1.4. Hypothesis

The hypothesis of this study is that a model developed for use in an entirely European hydrological setup with access to adequate data for flood simulation, can be adapted to simulate hydrologic behaviour of an extreme rain event for an area with less reliable data and different hydrologic conditions within a reasonable level of accuracy.

1.5. Thesis structure

Chapter 1 gives an introduction to the study, with motivation of the study, problem statement, objectives, research questions and the hypothesis. In **Chapter 2** literature is reviewed. **Chapter 3** introduces the study area and materials required. The methodology is discussed in **Chapter 4**. **Chapter 5** analyses the results. In **Chapter 6** conclusions are drawn and recommendations made.

2. LITERATURE REVIEW

2.1. Digital elevation model (SRTM)

In the year 2000 Jet Propulsion Laboratory's (JPL) Shuttle Radar Topography Mission (SRTM) was flown for ten days, mapping the world for topographic elevation for the entire footprint of the Shuttle's path (-54° to + 60° in altitude). The SRTM digital elevation model (DEM) has a resolution of 90m at the equator, and is provided by the Consultative Group on International Agricultural Research (CGIAR) in mosaicked 1° x 1° tiles. The SRTM data is available as 3 arc second (approximately 90m resolution) DEMs. The vertical error of the DEM's is reported to be less than 16m, (USGS, 2006). The data is projected in a Geographic (Lat/Long) projection, with the World Geodetic System 1984 (WGS84) horizontal datum and the Earth Gravitational Model of 1996 (EGM96) vertical datum [Description after (Farr and Kobrick, 2000; USGS 2006)].

2.1.1. SRTM data integrity assessment

The existence of regions without data (no-data regions) in a DEM can cause significant problems in using SRTM DEMs, especially in the application of hydrological models which require continuous flow surfaces. The data that is currently available from NASA/USGS contains someholes defined by "no-data" at locations where water or heavy shadow prevented the quantification of elevation. A correction for this involved the production of vector contours and points, and re-interpolation of these derived contours back into a raster DEM. For the Consultative Group on International Agricultural Research Consortium for Spatial Information(CGIAR-CSI) SRTM data product, a hole-filling algorithm was applied to provide continuous elevation surfaces. The interpolated DEM for the no-data regions was then merged with the original DEM to provide continuous elevation surfaces without no-data regions, (USGS 2006).

2.2. Rainfall estimation from space

2.2.1. TRMM-TMPA overview

The Tropical Rainfall Measuring Mission (TRMM) is a joint mission between NASA and the National Space Development Agency of Japan (JAXA) that serves to observe and understand how tropical rainfall affects the global climate. TRMM has five instruments: precipitation radar (PR), TRMM microwave imager (TMI), visible and infrared scanner (VIRS), cloud and earth radiant energy sensor (CERES), lightning imaging sensor (LIS). These instruments can all function individually or in combination with one another, (Huffman *et al.* 2001).

The TRMM Multi-satellite Precipitation Analysis (TMPA) is designed to combine precipitation estimates from various satellite systems and land surface precipitation from gauges. This primary merged microwave infrared product is computed at a 3-hourly temporal and 0.25° x 0.25° latitude–longitude spatial resolution (Huffman *et al.* 2007). The TMPA is computed as two products for TRMM. One product is an experimental real-time monitoring product that is produced nine hours after real time (TMPA_RT). A second product is a post-real-time research-quality product that becomes available aboutten to fifteen days after the end of each month (research product), (Huffman *et al.* 2001). The two products can be dowloaded at this link: http://gdata1.sci.gsfc.nasa.gov/daac-bin/G3/gui.cgi?instance_id=TRMM_3B42_Daily. In this research study the research product is used for rainfall estimation.

TMPA depends on input from two different sets of sensors. First, precipitation related passive microwave data are collected by a variety of low earth orbit (LEO) satellites, including the Microwave Imager (TMI) on TRMM, Special Sensor Microwave Imager (SSM/I) on Defense Meteorological Satellite Program (DMSP) satellites, Advanced Microwave Scanning Radiometer-Earth Observing System (AMSR-E) on *Aqua*, and the Advanced Microwave Sounding Unit-B (AMSU-B) on the National Oceanic and Atmospheric Administration (NOAA) satellite series. The second major data source for the TMPA is the window-channel (10.7μm) IR data that are collected by the international constellation of geo-synchronous earth orbit (GEO) satellites. This dataset includes grid-box-average Geostationary Operational Environmental Satellite (GOES) Precipitation Index (GPI) estimates computed from LEO–IR data recorded by the NOAA satellite series. These LEO–GPI data are used in the TMPA to fill gaps in the GEO–IR coverage [Description after Huffman *et al.* 2007].

The research TMPA makes use of a third set of data sources: The TRMM Combined Instrument (TCI) estimate, which employs data from both TMI and the TRMM precipitation radar (PR) as a source of calibration resulting in the TRMM Combined Instrument (TCI) 2B31 product (Haddad *et al.* 1997). The GPCP monthly rain gauge analysis developed by the Global Precipitation Climatological Center (GPCC) (Rudolf 1993), and the Climate Assessment and Monitoring System (CAMS) monthly rain gauge analysis developed by the Climate Prediction Center (CPC) (Xie and Arkin, 1997).

2.2.1.1. TRMM TMPA 3B42 v6 algorithm

Passive microwave fields of view (FOVs) from TMI, AMSR-E, and SSM/I are converted to precipitation estimates at the TRMM Science Data and Information System (TSDIS) with sensor-specific versions of the Goddard Profiling Algorithm (GPROF) (Kummerow *et al.* 1996; Olson *et al.* 1999). GPROF is a physically based algorithm that attempts to reconstruct the observed radiances for each FOV by selecting the "best" combination of thousands of numerical model generated microwave channel upwelling

radiances, (Huffman *et, al.* 1995). The associated vertical profiles of hydrometeors are used to provide an estimated surface precipitation rate. The microwave data are screened for contamination by surface effects as part of the processing, with marginal contamination denoted as "ambiguous." Passive microwave FOVs from AMSU-B are converted to precipitation estimates at the National Environmental Satellite, Data, and Information Service (NESDIS) with operational versions of the Weng and Grody (2002) and Weng *et al.* (2003) algorithm.

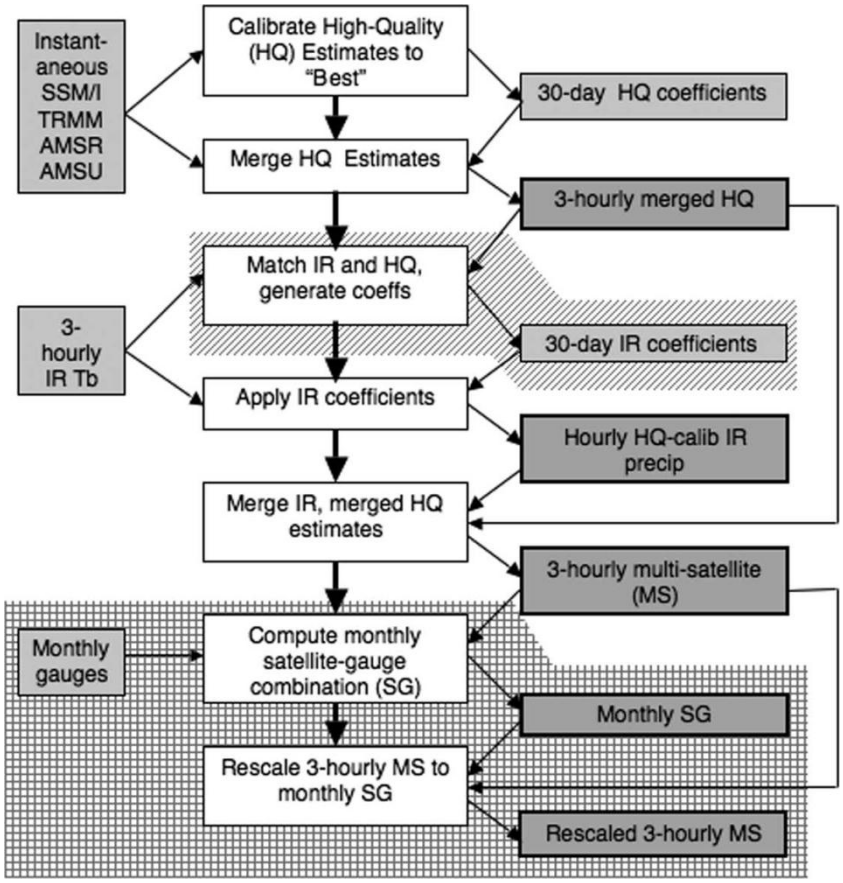

Figure 1: Block diagram for both the RT and research product algorithms *(Source Hufmann et al. 2006)*

The TMPA estimates are produced in four stages:

a) The microwave precipitation estimates are calibrated and combined,

b) Infrared precipitation estimates are created using the calibrated microwave precipitation,

c) The microwave and IR estimates are combined,

d) Rain gauge data are incorporated.

a. Combined high quality (HQ) microwave estimates

The TRMM Multi-Satellite Precipitation Analysis (TMPA; computed at fine intervals as 3B-42) inter-calibrates (to 2B31) and combines 2A-12, SSMI, AMSR and AMSU precipitation estimates (referred to as HQ see appendix 7.1). Passive microwave data are converted to precipitation estimates, and then each

data set is averaged to the 0.25° spatial grid over the time range ±90 minutes from the nominal observation time. These estimates are adjusted to a "best" estimate using probability matching of precipitation rate histograms assembled from coincident data. The algorithm takes the TCI as the calibrating data source. A TCI-TMI calibration is established and applied to TMI calibrations of the other sensors to estimate the TCI-calibrated values. The TCI-TMI relationship is computed on a 1°x1° grid for each month using that month's coincident data to accommodate the different climatologies of the two estimates (NASA-GSCF, 2011).

The TMI—AMSR-E and TMI—AMSU-B calibrations are set in the form of a single climatological adjustment for land and another for ocean. The rainfall estimates are calibrated for each satellite and audited for >40% "ambiguous pixels". Individual grids are populated by the "best" data from all available overpasses. The most likely number of overpasses in the 3-hr window for a given grid box is either one or zero. In the event of multiple overpasses, data from TCI, TCI-adjusted TMI, TCI-adjusted AMSR-E, and TCI-adjusted SSM/I are averaged together, and TCI-adjusted AMSU-B estimates are used if none of the others are available for the grid box [Description after (NASA-GSFC, 2011), (Acker and Leptoukh, 2007)].

b. Microwave-calibrated IR estimates

The research product uses two different IR datasets for creating the complete record of 3-hourly 0.25° gridded *Tb*'s. Each grid box's histogram is zenith-angle corrected, averaged to a single T_b value for the grid box, and plane-fit interpolated to the 0.25° grid. The CPC merged IR is averaged to 0.25° resolution and combined into hourly files as 30 min from the nominal time. Histograms of time–space matched combined microwave [high quality (HQ)] precipitation rates and IR *Tb*'s, each represented on the same 3-hourly 0.25°x0.25° grid, are accumulated for a month into histograms on a 1°x 1° grid.

By design, there is no precipitation when the 0.25°x0.25°-average T_b is greater than the local threshold value that matches the frequency of precipitation in the IR to that of the microwave. The histogram is specified by a fourth-order polynomial fit to climatology of coldest 0.17% precipitation rate points around the globe. In each grid box a constant is added to the climatological curve to make it continuous with the grid box's *Tb*-precipitation rate curve at the 0.17% *Tb*. Once computed, the HQ–IR calibration coefficients are applied to each 3-hourly IR dataset [Description after (NASA-GSFC, 2011), (Acker and Leptoukh, 2007)].

c. Merged microwave and IR estimates

The physically based combined microwave estimates are taken "as is" where available, and the remaining grid boxes are filled with microwave-calibrated IR estimates. This scheme provides the "best" local estimate, at the expense of a time series that displays heterogeneous statistics. Qualitatively, the algorithm

displays few noticeable data boundaries, in part due to the strong spatial variability that real precipitation systems exhibit (Acker and Leptoukh, 2007).

d. Rescaling to monthly data

It is highly advantageous to include rain gauge data in combination datasets (Huffman *et al.*1997). However on any time scale shorter than a month the gauge data are neither reported with sufficient density nor reported with consistent observational intervals to warrant direct inclusion in a global algorithm. In the rescaling process all available 3-hourly merged estimates are summed over a calendar month to create a monthly multi satellite (MS) product. The MS and gauge are combined to create a post real-time monthly SG combination, which is a TRMM research-grade product 3B43 (Acker and Leptoukh, 2007). The field of SG/MS ratios is computed on the 0.25°x0.25° grid (with controls) and applied to scale each 3-hourly field in the month, producing the version-6 3B42 product. The result is to provide the high resolution typical of satellite data combined with the small bias of gauge analyses over land. Detailed information on this algorithm is available at the link:
http://pps.gsfc.nasa.gov/tsdis/Documents/ICSVol4.pdf.

e. RT algorithm adjustments

The RT and research product systems are designed to be as similar as possible to ensure consistency between the resulting datasets. However, they have two major differences. The first difference is that the research product uses the TCI calibrator, whereas the RT uses the TMI estimates from TRMM.
Second the calibration month is taken as a trailing accumulation of 6 pentads (Acker and Leptoukh, 2007; Huffman *et al.* 2006). The TMI–SSM/I inter calibration and the microwave–IR coefficients are each recomputed at the end of each pentad, while there after there is inter-calibration of individual pentads.

2.2.1.2. TRMM-3B42 data integrity assessment

TMPA provides reasonable performance at monthly scales, although it is shown to have some bias due to lack of sensitivity to low precipitation rates over ocean in one of the input products namely AMSU-B, (Huffman *et. al.* 2006). The introduction of AMSU-B causes a low bias of almost 10% globally. At finer scales the TMPA is successful at approximately reproducing the surface observation based histogram of precipitation and reasonably detecting large daily events (NASA-GSCF, 2011).

In the present implementation of TMPA, the calibration is based on TRMM estimates. TMPA provides a calibration-based sequential scheme for combining precipitation estimates from multiple satellites, as well as gauge analyses where feasible, at fine scales (0.25° x 0.25° and 3 hourly). There is a minor discontinuity in the data record. The pre-February 2000 IR data covers the span 40 degrees north to 40 degrees south whilst post-February 2000 data cover 50 degrees north to 50 degrees south. The HQ data

sources are introduced at different points in the data record; therefore variations in HQ coverage occur throughout the record, increasing as time progresses [Description after Acker and Leptoukh, 2007].

2.2.1.3. Limitations of TRMM TMPA

The TRMM TMPA data have a strong physical relationship to the hydrometeors that result in surface precipitation. However each individual satellite provides a very sparse sampling of the time-space occurrence of precipitation. In addition there are significant gaps in the current 3-hourly coverage by the passive microwave estimates even when their combined spatial coverage is merged (NASA-GSCF, 2011).

2.3. Rainfall-runoff modeling

2.3.1. LISFLOOD

LISFLOOD was developed by the floods group under the Natural Hazards Project of the Joint Research Centre (JRC) of the European Commission (van der Knijff *et al.* 2008). The LISFLOOD model is implemented in the PCRaster Environmental Modelling language in a GIS environment, wrapped in a Python based interface (van Deursen *et al.* 1991). There exists a 'loose' coupling relationship between LISFLOOD, PCRaster and ArcGIS such that PCRaster and ArcGIS are used to pre-process the spatial data into the desired model input-file format and post-process the model (De Roo *et al.* 1989, De Roo (1996) and Kite *et al.* 1996). The Python wrapper of LISFLOOD enables the user to control the model inputs and outputs and the selection of the model modules. LISFLOOD runs on any operating system for which Python and PCRaster are available which currently include 32-bits Windows (Windows XP, Vista) and a number of Linux distributions.

LISFLOOD is a spatially distributed and physically-based flood simulation model that is specifically designed for channel and hydraulic routing as a consequence of extreme rainfall (De Roo*et al.* 1989, De Roo (1996)). The model simulates river discharge in a drainage basin as a function of spatial data influences on topography, soil properties, spatial precipitation and land cover. The model's primary output product is channel discharge whilst internal rate and state variables can also be written as output. All output can be written as grids, or time series at user-defined scales, points or areas.

The LISFLOOD model is made up of the following constituents:

a) a 2-layer soil water balance sub-model
b) sub-models for the simulation of groundwater and sub-surface flow
c) a sub-model for the routing of surface runoff to the nearest river channel
d) a sub-model for the routing of channel flow

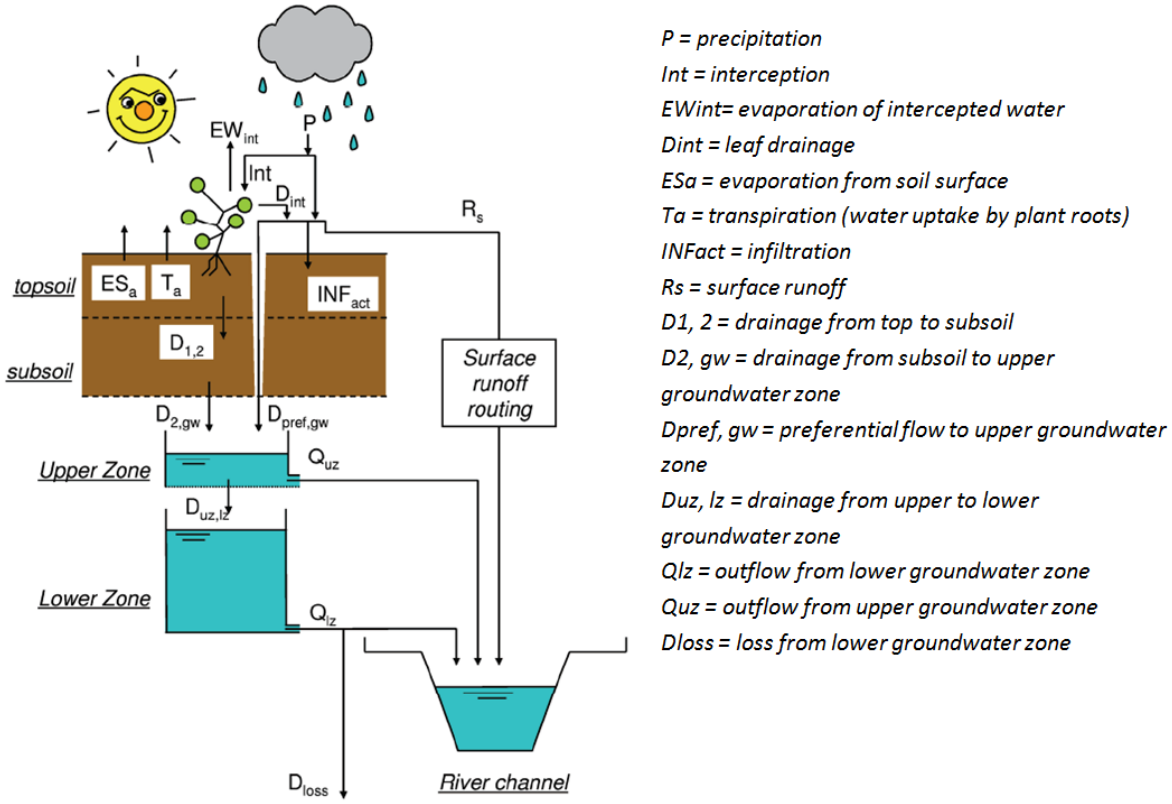

Figure 2: The LISFLOOD process (Source van der Knijff and de Roo , 2008)

The processes simulated by LISFLOOD are precipitation, interception, soil freezing, snow melt, infiltration, percolation, capillary rise, ground water flow and surface runoff. Surface runoff and channel routing are routed separately using a GIS based kinematic wave routing module as the Manning equation, (De Roo *et al.* 2000).

2.3.2. LISFLOOD input parameter maps

Land-use maps

2.3.2.1. GLOBCOVER land-use map (Africa)

The land use map of Cuvelai basin was extracted from the GLOBCOVER global map, at a spatial resolution of 300 meters. Details of the GLOBAL cover map are available at this link: http://geoserver.isciences.com:8080/geonetwork/srv/en/metadata.show?id=228. The objective of the GLOBCOVER / ESA initiative was to produce a global land-cover map for the year 2005-2006, using high spatial resolution (300 m) data acquired over the full year of 2005 by the MERIS sensor on-board the ENVISAT satellite. The classification module of the GLOBECOVER processing chain transforms the MERIS FR multi-spectral mosaics into a meaningful global land cover map with a legend defined and documented using the UN Land Cover Classification System (LCCS) (Fritz *et al.,* 2003).

LCCS was designed by the FAO (Food and Agriculture Organization) and UNEP (United Nations Environment Programme) as a hierarchical classification, which adjusts the thematic detail of the legend to the amount of information available to describe each land cover class. The Globcover land cover product's global legend is determined by the level of information that is available and that makes sense at the scale of the entire world. The level 1 legend, also called "global legend", meets this requirement, and was adopted for the section north-east of Africa where the Cuvelai is located.

2.3.2.2. CoRINE land-use map (Europe)

The LISFLOOD model to be adopted in this study uses the CoRINE land cover classification, which was developed specifically for European land use and land cover types. The land cover is available at this link: http://www.eea.europa.eu/publications/COR0-landcover. The CoRINE land cover nomenclature, [see Appendix 5 CORINE landuse nomenclature] comprises three levels: the first level (five items: artificial surfaces, agricultural areas, forests, semi natural areas and wetlands) indicates the major categories of land cover on the planet. The second level (15 items) is for use on scales of 1:500 000 and 1: 1 000 000. The third level (44 items) is applicable for projects on a scale of 1: 100 000. The land use classification system for the Cuvelai basin project is based on the broad level one classification.

2.3.2.3. Soils maps

Soils are generally classified in descending hierarchy from order, sub-order, great group, sub-group, family and series. Information on the details of this classification are available at this link: ftp://ftp-fc.sc.egov.usda.gov/NSSC/Soil_Taxonomy/tax.pdf . The dominant soils of Cuvelai basin fall into five taxonomy orders; namely acrisol, chernozem, luvisols, solonchacks and solonets as classified by the Food and Agriculture Organization, (FAO 1998). The Cuvelai basin soils maps were extracted from sheet 1 of the 1963 11th African regional joint project between the Commission for Technical Co-operation in Africa (CCTA), Inter-African Pedological Service and Institut Géographique. These maps are available at the following link: http://eusoils.jrc.ec.europa.eu/esdb_archive/EuDASM/africa/index.htm. The soil data used have a scale of 1: 5 000 000, however the quality of soil classification can be improved by using small scale maps of 1: 1000 000 ; 1: 250 000 or smaller scales if they are readily available and the project area is small. For the purpose of this research, the soils characteristics will be explored only at order level.

The soils data was available in FAO classification codes for Cuvelai basin. Detailed information on the classification codes is available at the following link: http://www.fao.org/wairdocs/ilri/x5546e/x5546e04.htm#. However, the LISFLOOD soils input maps are based on a United States Geological Survey (USGS) soils classification. Table 2 shows the adaptation of the FAO classes to the LISFLOOD-USGS classes through the relationship between the soil units and their related US taxonomy classes.

Table 1:FAO Soil Units and equivalent classification in Soil Taxonomy

FAO soil unit	FAO Symbol	United States Soil Taxonomy class
Acrisol	Ac	Ultisols
Chernozem	Ch	Borolls
Luvisols	Lv	Alfisols
Solonchacks	Sc	Salic Great Group
Solonetz	Sn	Natric Great Group

Source: http://en.wikipedia.org/wiki/World_Reference_Base_for_Soil_Resources

The table below shows the characterisation of the 5 soil classes at a depth of 100 centimeters from the topsoil.

Table 2: Characteristics of the Cuvelai dominant soil groups

FAO soil unit		Acrisol	Chernozem	Luvisols	Solonchacks	Solonetz
Classification		Fine, kaolinitic, thermic	Fine-silty, mixed	Fine, mixed, isohyperthermic	Coarse-loamy, carbonatic	Coarse-loamy
Parent material		Fluvial or marine sediments	Loess	Alluvium derived from igneous material over igneous rock	Mixed alluvium derived from andesite, limestone, and quartzite	Mixed alluvium derived from limestone, and quartzite
Land use		Forest land (not grazed)	Cropland	Cropland	Cropland	Grassland
Runoff class		High	High	High	Low	Medium
Drainage class		Poorly drained	Poorly drained	Average drainage	Well drained	Well drained
		Percentage weight of particles <2mm in diameter				
Grain size	Sand	20.4	23.3	25.7	50.4	39.2
	Silt	50.2	45.1	34.1	32.4	29.2
	Clay	29.4	31.6	40.2	17.2	37.9

Source (USDA 1999)

An acrisol is a clay-rich soil associated with humid, tropical climates, and often supports forested areas. The characteristic low fertility and toxic amounts of aluminium favour its use for silviculture, low intensity pasture and protected areas in many places. Chernozem are a soil common to grassland ecosystems. This soil is dark in color (brown to black) and has an A horizon that is rich in organic matter. Solonetz is a grassland soil where high levels of evapo-transpiration greatly exceeds precipitation input and cause the deposition of salts at or near the soil surface. These soils are common in floodplains with surface deposits

that are less than 3000 years old. Solonchak is a pale or grey soil type found in arid to sub-humid, poorly drained conditions. [Description after (UNESCO 1974; FAO 1998)]

PCRaster

PCRaster is a script-based environmental modelling computer language used for construction of iterative spatio-temporal environmental models. It is a raster-based Geographical Information System consisting of a set of computer tools for storing, manipulating, analysing and retrieving geographic information. The PCRaster Spatial Modelling language is a GIS capable of dynamic modelling. It runs on the interactive Nutshell and Map-edit platforms that support immediate pre- and post-modelling visualisation of spatio-temporal data. It has been extended with a kinematic wave approximation simulation tool to allow for physically based water flow modelling [Description after (Karssenberg 2002)].

Table 3: List of data types and domains for default cell representation in PCRaster.

	Description attributes	Domain	Example data type
boolean	boolean	0 (false), 1 (true)	suitable/unsuitable, visible/non visible
nominal	classified, no order	0...255, whole values	soil classes, administrative regions
ordinal	classified, order	0...255, whole values	succession stages, income groups
scalar	continuous, linear	-10exp(37)...10exp(37), real values	elevation, temperature
directional	continuous, directional	0 to 2 pi (radians), or to 360 (degrees), and -1 (no direction), real values	aspect
ldd	local drain direction to neighbour cell	1...9 (codes of drain directions)	drainage networks, wind directions

Source :http://pcraster.geo.uu.nl/documentation/pcrman/x181.htm#secdatbasemaptype

Data transfer to and from other GIS packages that support digitizing and scanning functionalities are implemented in PCRaster to cater for its simple functionalities. The central concept of PCRaster is a discretization of the landscape in space, resulting in individual cells of information. The different data formats have raster specific domains that support their conversion into code-readable maps (see **Table 3:** List of data types and domains for default cell representation in PCRaster.). Individual cells can receive and transmit information to and from neighbouring cells. Spatial data are stored in the database as PCRaster maps in a binary format used for representation of raster maps in PCRaster, (Karssenberg *et al.* 1997).

2.3.2.4. Advantages of PCRaster over other modelling computer languages

Compared with other computer languages such as C, Pascal, Java and C++ it has the advantage that it allows researchers to construct models by themselves in a relatively short period of time, even when they do not have experience in programming. Models constructed in the PCRaster language can easily be changed or extended and the results are immediately evaluated using visualisation routines linked to the language. This interactive approach of model building is not possible with models constructed in other low level computer languages such as C and Pascal. Changing such models mostly means rewriting the whole computer code, which can be time consuming programming. Most low level modelling languages need to be linked to separate software packages for visualisation of model output which results in clumsy data exchange.

2.3.3. Scriptive programming

PCRaster uses cartographic modelling which consists of operators that induce a change in the properties of the cells. The change in properties is calculated on the basis of dependency within cells (point operations) or between cells (neighbourhood operations, area operations, map operations). An extensive set of operators is currently available in the PCRaster system. This set of operators is a computer language designed especially for spatial and temporal analysis. The computer language is algebraic, thus the PCRaster operations can be applied and combined in the same way as algebraic calculations. In general an operation is done by typing:

pcrcalc *Result* = PCRasterOperator(*PCRasterExpression*)

pcrcalc	activates the PCRaster operation shell
PCRasterOperator	is a typical PCRaster operation resulting in the *Result*
Result	may be a map or a non-spatial value
PCRasterExpression	The map on which the operation is done

This map is called an *Expression* because it may be a map, but it may also be a PCRaster operation or a set of operations that result in a map or a non-spatial value. Several PCRaster operations may be nested in one command. Examples from the codes used in the Cuvelai project are:

pcrcalc ldd.*map* = lddcreate (dem.*map*,1E35,1E35,1E35,1E35) (2-2)

asc2map --*clone* area.*map* –N –a soildep.*txt* soildep.*map* (2-3)

Code (2-2) above is an example of generation of a local drain direction map (ldd.*map*) using PCRaster calculation based on the digital elevation model map (dem.*map*). The *.map* format is the only one compatible with the PCRaster software and its related interfaces. The figures 1E35 represent the total range of possible elevation cell values. Code number (2-3) is an example of generation of a soil depth map

soildep.*map* from the conversion of an ascii file read as a text file *.txt* which is the PCRaster compatible format. The codes used for the Cuvelai research project (see appendix 7.3) are based on nomenclature adopted from the LISFLOOD test catchment that is supplied with the sample codes for running the model (see appendix 7.2). The actual content of the input maps was adjusted to represent the Cuvelai basin conditions.

2.3.4. Rainfall-runoff models suited to the hydrology of Africa

One of many objectives of rainfall-runoff modeling is to generate a long representative time series of stream flow volumes from which water resource estimation and management schemes can be designed. Several rainfall-runoff models have been developed and applied with varying degrees of success in different parts of Africa's large and ungauged river basins and catchments. The following case studies were analyzed prior to the selection of LISFLOOD model as most suited for the research study:

2.3.4.1. Simplified Precipitation and Lumped Algorithms for Stream-flow Hydrographs (SPLASH)

The SPLASH model is a conceptual daily rainfall-runoff model designed for use in large river basins. It came about as a result of a literature survey conducted by van Biljon, (2007) to increase his understanding of different models and to determine the availability of rainfall-runoff models suited to hydrologic conditions in Africa. The focus was on reasonably simple models in terms of structure, input and parsimony of parameters. Biljon (2007), identified the Nedbor-Afstromnings-Model-System 11 (NAM-S11) model developed by Danish hydrologists for flood prediction in which overland flow, interflow and base flow are totally dependent on the status of soil moisture. The NAM-S11 model provided the opportunity for further investigation and the result was the development of SPLASH, a simplified model with alterations to the original algorithms by modification to better suit Southern African hydrological conditions by excluding snow and ice formation.

The model was tested using data of two South African rivers:

- Klaserie river at Fleur de Lys (catchment area 136 km^2) with mean annual rainfall <1200mm
- Vaal river at Standerton (catchment area 8192 km^2) with mean annual rainfall of 650mm

The model was fairly successful as it used simplified precipitation and lumped algorithms for stream flow hydrographs. However, the results could be improved by making the parameterization distributed, than treating it uniformly to accommodate the spatial variability of the larger river basin.

2.3.4.2. Soil and Water Assessment Tool (SWAT)

SWAT is a distributed rainfall-runoff model. A study of the applicability of SWAT in Tanzania was carried out by Ndomba *et al*, (2008). The study area was Kikuletwa sub-catchment in Pangani river basin (north-east Tanzania). Previous researchers argued that the applicability of such a hydrologically complex model requiring many parameters would be impractical over a data scarce region such as the study area. Ndomba

et al, (2008) argued that developing countries do not have the financial and human capacity to develop new models, so it is beneficial to customize models working in other parts of the world, to fit the needs of such areas as the study area.

The study found out that the same set of important parameters can be identified using observed or without data (no data). These parameters are: curve number 'CN2", surface lag Day "Surlag", depth of water in shallow aquifer "GWQMN"and percentage slope "SLOPE". Parameters like soil evaporation coefficient "ESCO", available water capacity "SOL-AWC", base flow recession coefficient "ALPHA-BF", effective hydraulic conductivity "Ch- K2", slope sub-basin "SLSURBBSN" and depth of water in shallow aquifer "GWQMN" were identified as slightly less important parameters. The rest of the parameters did not influence model output. This result suggested that the SWAT model can be used in ungauged catchments for identifying hydrological controlling parameters. Calibration using manual and expert knowledge approaches was difficult for the research team; however, the modeling exercise suggested that using adequately processed and reliable spatial rainfall data can improve the results of the study.

A parallel study was carried out by (Mulungu and Munishi 2007)) to model the Simuyu River catchment in Tanzania using SWAT. The model inputs were based on high resolution data from Landsat Thematic Mapper (TM) of 30m spatial resolution and 90 m DEM. However, a low level of performance was achieved. This indicated that other factors than the spatial land data are greatly important for improvement of flow estimation by SWAT in the case of Simuyu, and probably in general. A huge computational resource requirement also decreased the performance of this model.

2.3.4.3. MIKE-SHE model

The MIKE-SHE model was tested in Senegal by Stisen *et al.* in (2008). The study investigated the potential of applying remote sensing (RS) based input data in a hydrological model for the 350,000 km^2 Senegal River basin in West Africa. By utilizing remote sensing data to estimate precipitation, potential evapo-transpiration (PET) and leaf area index (LAI) the model was driven entirely by remote sensing based data and independent of traditional meteorological data. The remote sensing retrievals were based on data from the geostationary METEOSAT-7 and the polar orbiting advanced very high resolution radiometer (AVHRR). The distributed hydrological model MIKE SHE was calibrated and validated against observed discharge for six individual sub catchments during the period 1998-2005. The model generally performed well for both root mean square error (RMSE), water balance error (WBE) and correlation coefficient (R^2).

For comparison a model based on standard meteorological driving variables was developed for a single sub catchment. The two models based on remote sensing and conventional data, respectively, exhibited similar model performances. Simulated actual evapo-transpiration (AET) was compared to measurements

at point scale and good agreement was obtained both on an event basis and seasonally. The potential for driving large scale hydrological models using remote sensing data was clearly demonstrated and further emphasized by the presence of long time records and near real time accessibility of the satellite data sources.

2.3.4.4. Pitman Model

The Pitman model is a conceptual model consisting of storages linked by functions designed to represent the main hydrological processes within a catchment scale. It has interception, impervious area runoff, catchment absorption and surface runoff, soil and ground water runoff and evaporative loss functions. Kapangarwizi in 2007 attempted to address the need to model ungauged catchments of African hydrological conditions. To achieve this he developed a conceptual framework for the physical interpretation of the Pitman parameters. He also developed equations for the direct estimation of model parameters from physical basin properties, to generate sets of parameters for the model in selected basins in southern Africa. The general conclusion was that the Pitman model can be satisfactorily applied to semi-arid areas with ungauged catchments.

3. STUDY AREA AND MATERIALS

3.1. Description of the study area

3.1.1. General description

The Cuvelai River originates in Angola, and its catchment lies between the Cunene basin in the west and the Okavango basin in the east. The Cuvelai River enters Namibia as a 130 km wide delta of ephemeral watercourses, which converge to terminate in the Etosha Pan, (Contreras, Boer et al. 2008). The Cuvelai Basin spans from south Angola intothe densely populated north central part of rural Namibia. The basin has an approximate total area of 164000km².

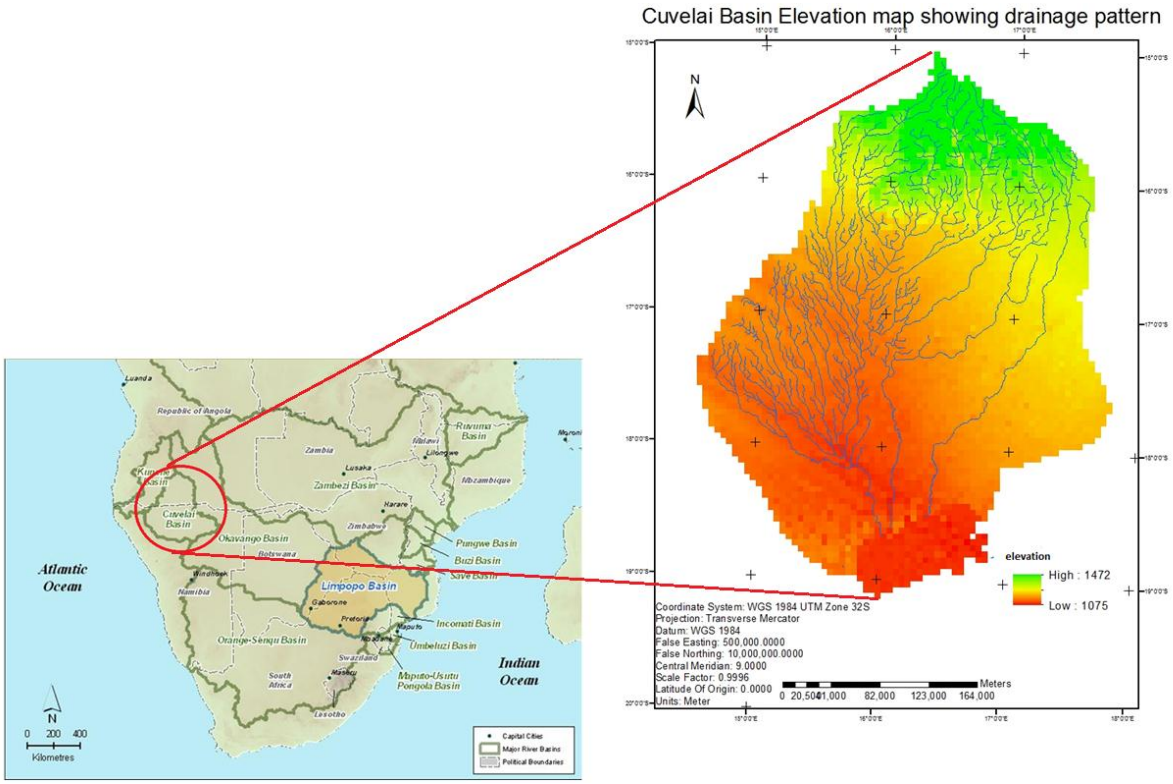

Figure 3: Location of Cuvelai Basin
(Source: http://www.limpoporak.com/en/river/geography/basins+of+southern+africa.aspx)

3.1.2. Historical information

Seasonal downpours bring a rush of water to the Cuvelai basin, supplementing the basin's few permanent water features. Annually Efundja (the Oshiwambo name for the annual floods coming from Angola) fills the shanas (floodplains) in the northern regions, (NHS, 2009). The arrival of the flood is much anticipated as it brings fish, restores grazing capacity and ensures water reserves for the dry months after the rainy season. However in 2009, the seasonal floods were extreme, forcing evacuations in communities throughout the basin. 147 lives were lost , more than 30 000 people were displaced and over (USD) $500 millions of dollars worth of property and agricultural produce was destroyed (NHS, 2009).

The floods led to the development of new hydrological conditions and drainage patterns as dried out lakes filled up (lake Liambezi) and fossil channels started to flow (Selinda river connecting to Kavango river), (NHS, 2009).

Traditionally, rainfall is measured using rain gauges at ground stations, but in the Cuvelai basin rain gauges are few and poorly distributed. Rainfall-runoff modeling using satellite based rainfall estimations provides an opportunity to easily simulate the response of a watershed, thus providing an option for better water resources management particularly in Arid and Semi-Arid Areas (ASAL) regions of Sub-Saharan Africa (SSA), Kinoti *et al.,* (2010). Estimates of satellite based accumulated rainfall have to be made to fill the no-data gap and better understand the spatio-temporal relationship between rainfall inputs and floods.

Current efforts are being made by external partners such as the German Aerospace Center (DLR) to provide data in the form of flood maps for monitoring and evaluation of the extents of inundation. The figure below shows some images of the Cuvelai river taken by Terra SAR on the 28th of March 2009 and 29th of April 2009 respectively. In this image the recession of the inundation is observed after a period of one month from the occurrence of the flood event.

Figure 4: Terra SAR images of flooding in Cuvelai river in 2009
Source: http://earthobservatory.nasa.gov/NaturalHazards/view.php?id=37730

Flood levels for the 2010-2011 rainfall season in north-central Namibia in the Cuvelai basin were recorded at eight centimetres higher than in the 2009-2010 flood season, setting a new record for the area where about one million people (almost half of Namibia's population) live (Inter Press Service, 2011). The north-central area is a source of livelihood for a majority of rural Namibia, as it offers subsistence through farming and fishing in the wetlands. There are predictions that the frequency and extents of flooding will increase in the Cuvelai basin, therefore it is important to harness all possible technology to develop early warning systems such as flood forecasting (NHS,2009).

3.1.3. Topography and lithology

The Cuvelai basin lies on the western edge of the Central African Plateau, at around 1,000 m in elevation. The basin has a very flat topography and a shallow gradient to the south. The area is mostly flat, but gains elevation towards the south, where it reaches its highest point in the Waterberg mountains (1,857 m) (Barnard 1998). The soils of the Cuvelai basin contain luvisol basement sediments. These include acrisolic soils around the Etosha Pan, weakly developed shallow soils of arid origin to the south, and solonetzic and solonchack soilsto the north. The natric soils of the Etosha area are shallow, alkaline, and high in water soluble salts while poor in both phosphates and nitrogen (le Roux 1980).

3.1.4. Climate

The Cuvelai basin has a predominantly semi-arid to arid climate with low and irregular rain events followed by high levels of evaporation from very high air temperatures (Contreras, Boer et al. 2008). The hallmarks of this area are marked drought and aridity from May to October switching to floods during the second half of the rainy season from January to April (DWAF, 2008). Rain falls mainly in summer (November to March) and precipitation occurrence and amount increases slightly from west to east and decreases greatly from north to south within the basin. More recently rainfall patterns and quantities are unpredictable, and the Cuvelai basin now experiences changing dry and rainy seasons with extremes in between droughts and flooding (DWAF, 2008).

3.1.5. Hydrology

Cuvelai's drainage system, which straddles the border between Angola and Namibia, includes the ephemeral shallow streams of inter-linked water courses locally known as oshanas (grass covered temporary water channels) and pans (circular shaped depression temporarily holding water, often endorheic). There are five perennial rivers around the basin, namely the Kunene, Kavango, Zambezi and Kwando-Linyati in the north and Orange in the south. There are several small rivers on the west of the basin that carry water only for short periods of time after the rains, (van der Waal 1991). The average annual rainfall is 400-550 mm and falls mostly from December to March, which contributes, along with high floods, to the surface water flow of the basin, (Barnard 1998).

3.2. Materials

3.2.1. Satellite data products

3.2.1.1. TRMM 3b-42 rainfall product

The TRMM daily or climate rainfall products, referred to as the level 6 products, are derived from a combination of the TRMM level 2 products and instantaneous rainfall estimates corresponding to the satellite snapshot views. The availability of multiple rainfall products from the various TRMM rainfall sensors is due to the fact that each one has various strengths and weaknesses, and these are combined to

make a single product that is more accurate. The combined instrument rain calibration algorithm (3B-42) uses an optimal combination of 2B-31, 2A-12, SSMI, AMSR and AMSU precipitation estimates (referred to as High Quality (HQ)), to adjust IR estimates from geostationary IR observations. Near-global estimates are made by calibrating the IR brightness temperatures to the HQ estimates. The 3B-42 estimates are scaled to match the monthly rain gauge analyses used in 3B-43. The output is rainfall for 0.25 x 0.25 degree grid boxes every 3 hours, which is then aggregated to average daily rainfall [Description after, Huffman *et al.* (1995, 2007)].

Table 4:TRMM 3B42 data characteristics

TRMM 3B42 Characteristics	
Temporal Coverage	Start Date: 1998-01-01; Stop Date: -
Geographic Coverage	Latitude: 50°S - 50°N; Longitude:180°W - 180°E
Temporal Resolution	3-Hourly, Daily
Horizontal Resolution	0.25° x 0.25°; nlat = 400, nlon = 1440
Average File Size	Compressed: ~285 KB; Original: ~4.5 MB
Available formats	Ascii, HDF, NetCDF, Google Earth KMZ

(Source *Acker and Leptoukh 2007*)

3.2.1.2. TRMM Online Visualisation and Analysis System (TOVAS)

Giovanni is an interactive web-based application developed by the GES DISC that provides a simple and intuitive way to visualize, analyse, and access and download vast amounts of Earth science remote sensing data, (Theon 1994). Giovanni is comprised of a number of interfaces, called instances, each tailored to meet the needs of different Earth science research communities. One such interface is the TRMM/TOVAS system, under the hydrological interfaces group. TOVAS stands for the "TRMM Online Visualization and Analysis System", where TRMM is the acronym for the Tropical Rainfall Measuring Mission. The TRMM-TMPA data are available for free download at the following link: http://disc.sci.gsfc.nasa.gov/giovanni.

The product 3B42 v6 is available from GIOVANNI TOVAS in four formats: HDF, NetCDF (NCD), ASCII (available only when the array size is within about half-million points), and Google Earth KMZ. The product is available as either 3 hourly rainfall data or composite daily rainfall data with 25 kilometerspatial resolution.

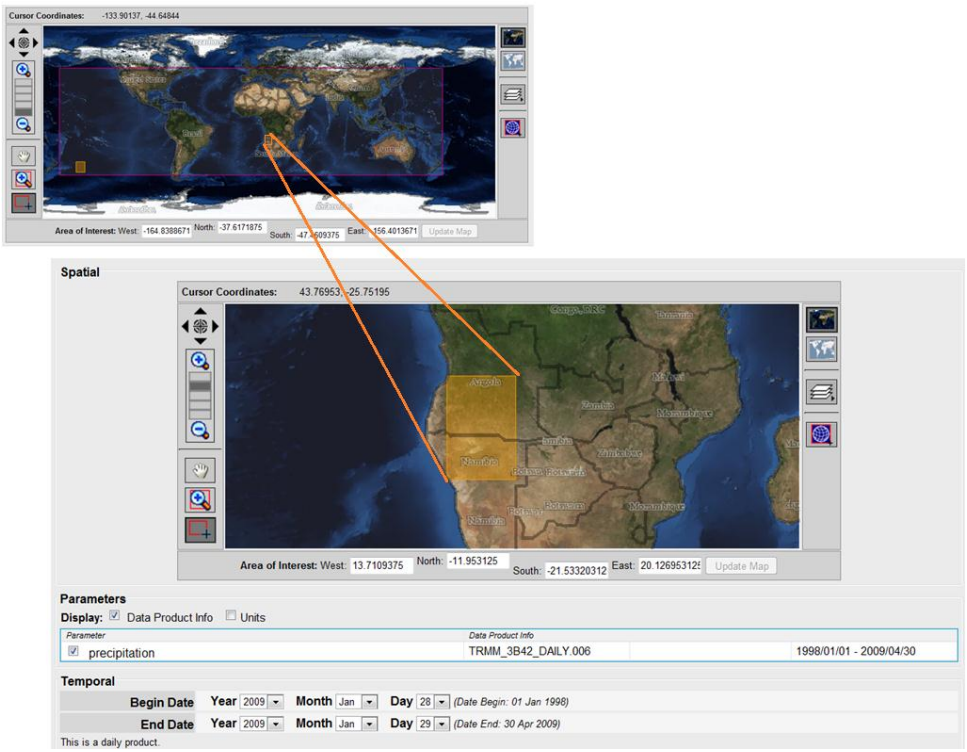

Figure 5: GIOVANNI TOVAS interactive interface
(Source: http://gdata1.sci.gsfc.nasa.gov/daac-bin/G3/gui.cgi?instance_id=TRMM_3B42_Daily)

3.2.1.3. MODIS Leaf Area Index

The algorithm uses sun and view angle directions of the MODIS satellite to find LAI values given, Bidirectional Reflectance Factor (BRF) for each MODIS band, band uncertainties, and six biome land cover classes, (Ranga *et al.* 2000). The algorithm is executed on a daily basis.

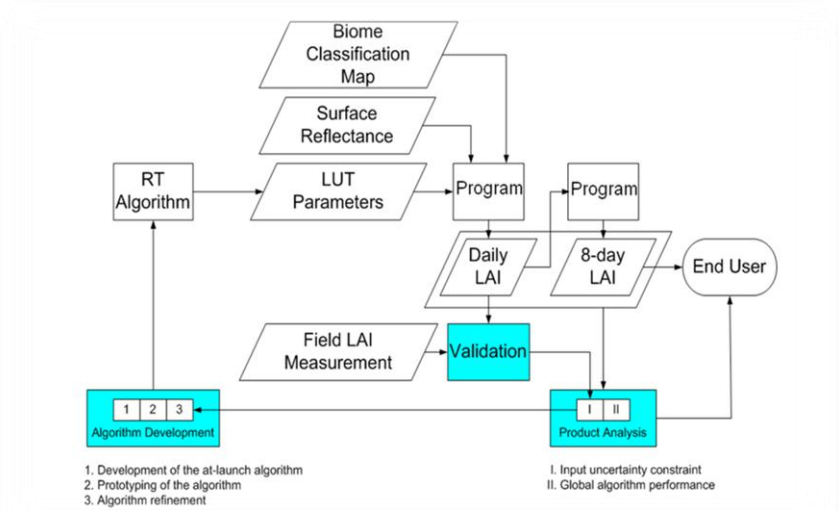

Figure 6: Algorithm for MODIS LAI data (Source: http://www.ntsg.umt.edu/project/modis#data-product)

The processing is done by NASA and daily LAI values are composited over an eight day period. The products are distributed from the EDC Data Center as 1 km 8-day products. Detailed information about the MODIS product is available at the following link:

https://lpdaac.usgs.gov/lpdaac/products/modis_products_table. The flow chart overleaf shows a summary of the process. The closed loop between product analysis, validation and algorithm refinement is a key element for improving product quality in each successive re-processing of LAI.

An inspection of the temporal variations in LAI give rise to the observation that LAI increases, slightly, and in areas such as north-east of the basin, and remain low in the more 'arid' sections in the middle parts following throug to the Etosha pan.

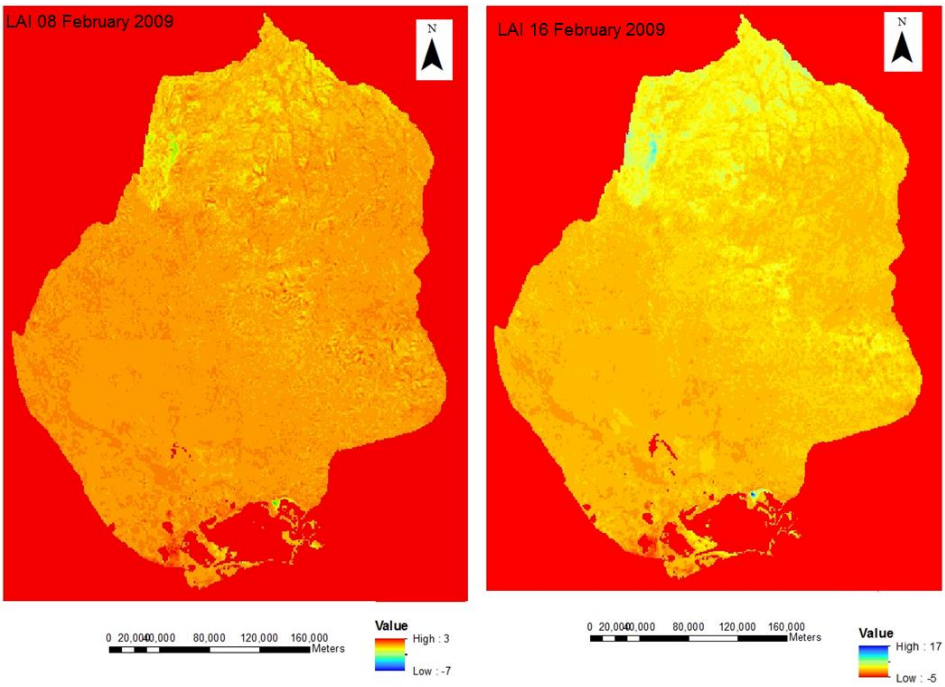

Figure 7: Difference map for Lai 08 February and Lai 18 February

There appears to be an increase in LAI in the North west region of the basin. This is because it is an area of high agricultural activity, so crops are at various stages of development. The LAI also increases markedly south east of the basin, in a single position, just above the pan. This is the location of a thriving wetland. In generall the LAI has slight increases during the 40 day run of LISFLOOD.

3.2.1.4. GLOBECOVER Land use

The GLOBCOVER project was launched 2004 as an initiative of ESA. It has now evolved to an international collaboration between ESA, FAO, UNEP, JRC, IGBP and GOFC-GOLD. The objective of GLOBCOVER is to produce a global land-cover map for the year 2005, using as main source of data the fine resolution (300 m) mode data from MERIS sensor on-board ENVISAT satellite, acquired over the full year 2005. The GLOBCOVER product intends to complement and update other existing comparable global products, such as the global land cover map for the year 2000 (GLC 2000) with a resolution of 1 km produced by the JRC. Appropriate approaches for the validation of the land cover products are planned to be defined in consultation with Centre for Earth Observation Science (CEOS).

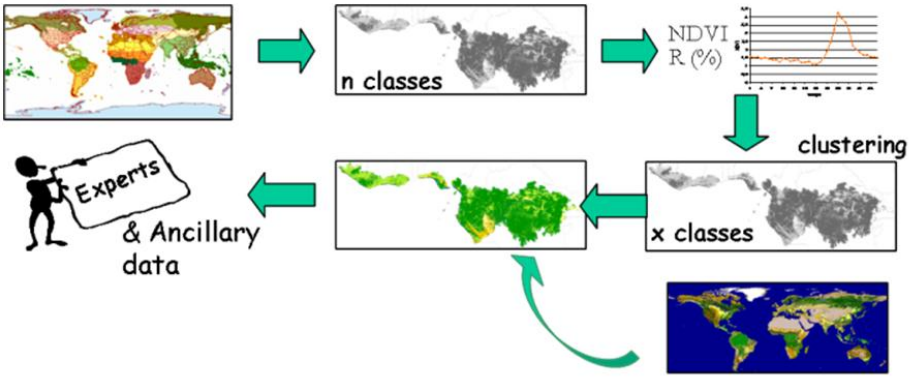

Figure 8: GLOBCOVER landuse classification process
Source: http://postel.mediasfrance.org/en/BIOGEOPHYSICAL-PRODUCTS/Land-Cover/

3.2.1.5. Soils

The Cuvelai basin soils map was extracted from the Africa soils database which in itself is a product of the global soils database (digitized by the ESRI Corporation) from the 1974 FAO/UNESCO Soil Map of the World at 1: 5,000,000 scale. The legend of the soil map of the world comprises an estimated 5000 different mapping units, consisting of soil units or associations. The legend of the FAO/ UNESCO Soil Map of the World is composed of 106 soil unit classes (http://www.lib.berkeley.edu/EART/fao.html), (FAO/UNESCO 1974). In the UNEP/GRID version, the dominant soil group is identified (for example 'Acrisols' when the dominant Acrisols unit is not known). A non-homogeneous map unit is composed of a dominant soil and associated soils, with the latter covering at least 20 per cent of a given area. Important soils covering less than 20 per cent of a given area are added as inclusions, (FAO/UNESCO 1974).

3.2.1.6. Evapo-transpiration (ET)

The evapo-transpiration (ET) product is derived from SEVIRI radiometer aboard the MSG satellite at 3 kilometer spatial and 30 minute temporal resolution. Two ET products are produced: the instantaneous ET and the daily ET. The ET algorithm targets the quantification of the flux of water vapour from the ground surface (soil and canopy) into the atmosphere using input data derived from MSG satellite. The product used for Cuvelai basin was taken from Southern Africa (SAFr) geographical area within the Meteosat disk, covering the African continent south of the equator. Detailed information on the ET product is available at the following link: http://landsaf.meteo.pt.

The procedure follows a physical approach which can be described as a combination of the Soil-Vegetation-Atmosphere Transfer (SVAT) scheme and Tiled Land-Surface Scheme (TESSEL) land surface model. For simplification SVAT is modified to accept satellite remote sensing derived data combined with data from numerical weather prediction (NWP) as forcing. Detailed information on the TESSEL model is available at the following link:
http://www.ecmwf.int/research/EU_projects/GEOLAND/CTESSEL/index.html

The TESSEL land surface model is a physical model based on soil moisture. In practice, the combined model is run on MSG images. Each pixel is considered as a mix of homogeneous entities "tiles" representing a particular coverage type (bare soil, grassland, crops, and forests). Some parameters are defined at the pixel level and are thus shared by all the tiles composing the pixel, while others are defined at the tile level, most of them being extracted from the ECOCLIMAP database (Masson *et al.* 2003). The resulting ET value for each pixel is obtained through the weighted contribution of each considered tile in the pixel [Description after (Gellens-Meulenberghs *et al.* 2007)].

3.2.1.7. Elevation SRTM

The first release of Shuttle Radar Topography Mission (SRTM) data was provided in 1-degree digital elevation model (DEM) tiles from the USGS in 2003. The data was released continent by continent, as and when the data was processed by NASA and the USGS. The global data is available at 3-arc seconds (approximately 90m at the equator) at the following link:
ftp://e0srp01u.ecs.nasa.gov/srtm/version2/SRTM3/.

The digital elevation model from SRTM follows a four step production process: The first stage involves importing and merging 1-degree tiles into continuous elevation surfaces in Arc GRID format using the Arc/Info AML model. The second process fills small holes iteratively, and the surface is cleaned to reduce pits and peaks. The third stage interpolates through the holes using a range of methods based on the size of the hole, and the landform that surrounds it. The final step is the merging of the original DEM with the interpolated DEM for the no-data regions to provide continuous elevation surfaces without no-data regions. [Description after USGS 2006]

3.2.1.8. Land Surface Temperature (LST)

The temperature of land surfaces is an essential parameter that drives the water balance. METEOSAT is the only satellite that provides infrared measurements over Africa and Europe that resolves the diurnal wave of land surface temperature. Land surface temperature (LST) for this project is retrieved from METEOSAT SEVIRI thermal infrared channel satellite images using a neural network. The images have a spatial resolution of 5km at nadir, and a 30 minute temporal resolution.

The LST is determined by interpolation of the satellite measurements for profiles around the current pixel and horizontal interpolation of the atmospheric correction at the surrounding pixels. The atmospheric correction coefficient is determined using a reference within the image. The reference is obtained from the driest pixels, which have the highest planetary temperature over global radiation ratio. It is assumed that these pixels have zero evapotranspiration and thus sensible heat flux equals net radiation.A neural network

is used to speed-up this procedure. The average surface temperature is obtained by averaging the noon and midnight surface temperature.

3.2.1.9. Quality assessment

The use of satellite data as input in a hydrological model requires accuracy of the highest level possible. The datasets described earlier have had accuracy checks done to ensure that there is minimal error due to the actual input data itself. The LISFLOOD model is very sensitive to 'missing values' in the input maps (van der Knijff and de Roo 2008). The table overleaf shows a summary of the accuracy check done on the satellite data before use in the model.

Table 5: Quality assessment of satellite data

Satellite imagery	Quality assurance / accuracy levels
MODIS Leaf Area Index	Science data quality flag was inferred as 'passed'on 17/04/2002, but the following is to be observed: Over inland water bodies (rivers, lakes, etc...) surface reflectance inputs and VI values are not be stable and should be used with caution. Users are advised to examine the per-pixel product quality to screen poor data before applying it to project-applications, science, and research. http://landweb.nascom.nasa.gov/cgi-bin/QA_WWW/detailInfo.cgi?prod_id=MYD13Q1&ver=C5
GLOBECOVER Land use	The final product has a relative RMSE of <50 mand <80 m absolute RMSE. Corrections have been implemented to diminish the influence of the atmosphere.In orderto minimise the bi-directional reflectance effects a simple composition averaging (BRDF correction) was used. http://due.esrin.esa.int/prjs/Results/20110202183257.pdf
Evapo-transpiration (ET)	The error estimate is the most general quality indicator operationally delivered by the algorithm. Automatic quality control (QC) is performed on each product and the quality information is provided on a pixel basis. Dark pixels (uncertainty < 0.1), green (uncertainty 0.1-0.15), yellow pixels (uncertainty 0.15 -0.20), red pixels correspond to unusable areas. http://www.earsel.org/symposia/2009-symposium-Chania/09EARSEL_garciaharoetal_LSASAF.pdf
Precipitation TRMM v6-3B42	All TRMM products are provided with random error estimates. The data record have gaps in the record dueto processing errors and down time on receivers related to satellite imagery shortcomings. TMI error detection and correction is done by deleting all pixels with non-physical Tb and local calibration errors. ftp://precip.gsfc.nasa.gov/pub/trmmdocs/3B42_3B43_doc.pdf
SRTM DEM	The SRTM DEM has an average error of 8 m as opposed to 20 m for the TOPO DEM. In area specific studies around the world systematic errors were identified in the SRTM data, related to aspect. The errors were found to be highest in northeast-facing slopes, attributed to the effect of incidence angle of the original radar images used to produce the SRTM DEM. http://srtm.csi.cgiar.org/PDF/Jarvis4.pdf
Land surface temperature (LST)	Errors in the data such include individual pixel count errors, missing parts of scan-lines, wrong geo-location and missing periods. There are also unknown errors in ECMWF re-analysis. http://postel.mediasfrance.org/IMG/pdf/CSP-0350-ATBD_LST-I1.00.pdf

4. METHODS

4.1. Data preprocessing

The project involved pre-processing of the satellite images to change the projection and size of each raster layer. Most of the global or regional data was in decimal degrees, lat-long projection, at 1km spatial resolution. The temporal resolution for the non-daily data such as the decadal data was not a restriction as LISFLOOD accepts map stacks in the respective input files code.

The re-projection co-ordinate system used to unify the usability of all the raster datasets and shape files data for the entire project are: UTM, datum WGS84, ellipsoid WGS1984 in zone 33 of the southern hemishpere. The whole Cuvelai catchment falls into zone 33, detailed information is available on this link: http://www.unitar.org/unosat/node/44/1168. A shape file of the Cuvelai basin boundary Cuvelai.*shp* was created for use through out the entire raster data related boundary definitions for the pre-PCRaster data preparation in ArcGIS. All the Cuvelai data was altered to replicate the formats of the unnamed test catchment data and input maps made available together with the code to assess the functionality of LISFLOOD upon installation.

Table 6: Example of map stack for LAI data in LISFLOOD

Time step	Map name
1	lai00000.001
2	-
-	-
19	-
20	lai00000.024
-	-
31	-
32	lai00000.032
-	-

(Source: van der Knijff and de Roo, 2008)

4.1.1. Interpolation by Inverse Distance Weighting (IDW)

Inverse distance weighted (IDW) interpolation determines cell values by using a linearly weighted combination of a set of points. This method assumes that the variable being mapped decreases in influence with distance from its sampled location. The characteristics of the interpolated surface are also controlled by altering the input points used in the calculation of each output cell value. Using a variable search radius, the number of points used in calculating the value of the interpolated cell is specified. This makes the radius distance vary for each interpolated cell, depending on how far it has to search around each interpolated cell to reach the specified number of input points. Every measured point that falls within the radius specified will be used in the calculation of each interpolated cell.

IDW interpolation of the TRMM_TOVAS 3b42 rainfall maps for this study was carried out using the spatial analyst tool in ArcMAP software. The specifics of the parameters defined are: search radius (12), output cell size (5000meters), power (2), and the z-value field (value = rainfall in mm/day). For the purpose of this chapter, all instances referring to interpolation should be assumed to have used these specifics and were carried out in ArcMAP.

4.1.2. Resampling

This study involved a lot of processing between multiple datasets, therefore it is critical to ensure that all the different pre-LISFLOOD maps have the same cell resolution. The three techniques for determining output values are nearest neighbor assignment, bilinear interpolation, and cubic convolution. Nearest neighbor assignment does not change any of the values of output cells from the input raster dataset therefore it is the resampling technique of choice for discrete (categorical) data. Since the output cell values remain the same, nearest neighbor assignment is also ideal for nominal and ordinal data, where each value represents a class, member, or classification (categorical data such as a land-use, soil, or forest type).

In this study, the nearest neighbor assignment resampling technique is used. This is because it is applicable to both discrete and continuous value types, while the other resampling types: bilinear interpolation and cubic convolution are restrictive in their applications since they are only applicable to continuous data. Any instances referring to resampling of raster datasets in this study used the ArcMAP data management tool's raster processing operator. The specifications of the resample are: output cell size (5000 meters), resampling technique (nearest neighbour).

4.1.3. Reclassification

The reclassification tools change cell values to alternative values using a variety of methods. There are several approaches to reclassifying data, namely by lookup option, by a range of values such as by ascii file or tables and by intervals such as slicing.

This study required reclassification of several datasets to match the LISFLOOD associated data format and look-up tables. For all datasets referred to as having been reclassified, the procedure was done in ArcMAP using the reclassify operator from the reclass option in spatial analyst tools and reclass by either slicing or natural breaks was used depending on the adjustment needs of the dataset. Individual adjustments made to original data classes have been outlined in the literature review and are further explained in the respective sections below for LAI, land use and soils data sets.

4.1.4. Satellite data products

4.1.4.1. MODIS Leaf Area Index

The original LAI raster files for the African continent were read directly in ArcMap because of their *.tiff* format. The Cuvelai basin was extracted from the continent data using the extract by mask ArcMAP spatial analyst tool. The Cuvelai LAI raster datasets were then re-projected from decimal degrees geographic co-ordinate system to UTM projection system, then reclassified to match the LISFLOOD system. The reclassified raster datasets were resampled from the 1km spatial resolution of origin to 5km resolution [the pixel size selected for running the model]. The resampled LAI raster data were converted from *.grid* raster to *.txt* for use in PCRaster. The new maps prefixed '*lai'* were created using the Nutshell interface of PCRaster to convert the lai00000.001.*txt* file into the final product lai00000.001.*map* using the 'asc2map' command.

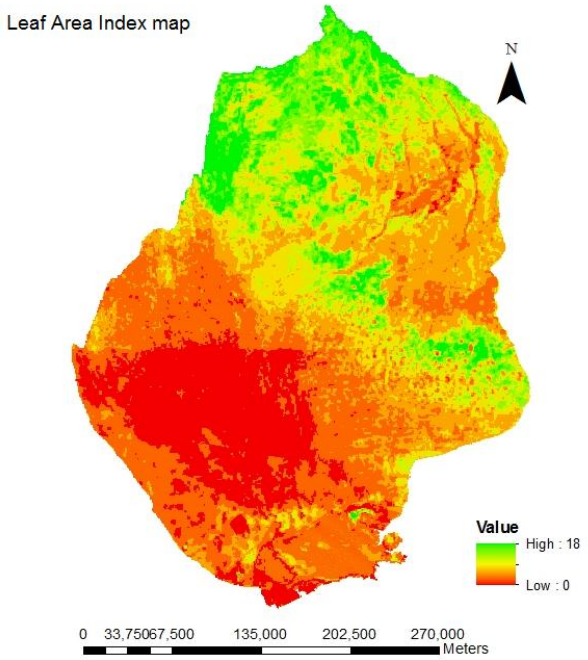

Figure 9: LAI 24 February 2009

There is generally high leaf area index in the upper parts of the catchment. This is because it is an area of forests and peri-urban agriculture. The grasslands and shrublands on the north-east seem to have very low LAI recorded.

4.1.4.2. GLOBECOV Land use

The project area was extracted from the global land cover map of using the Cuvelai basin boundary Cuvelai.*shp* created in earlier steps in the ArcMAP spatial analyst tools. The raster-based soils land use files were converted to polygons using the raster to polygon tool. The newly created land use polygon dataset was reclassified from the GLOBCOVER land cover classes to match the CoRINE classes used by LISFLOOD.

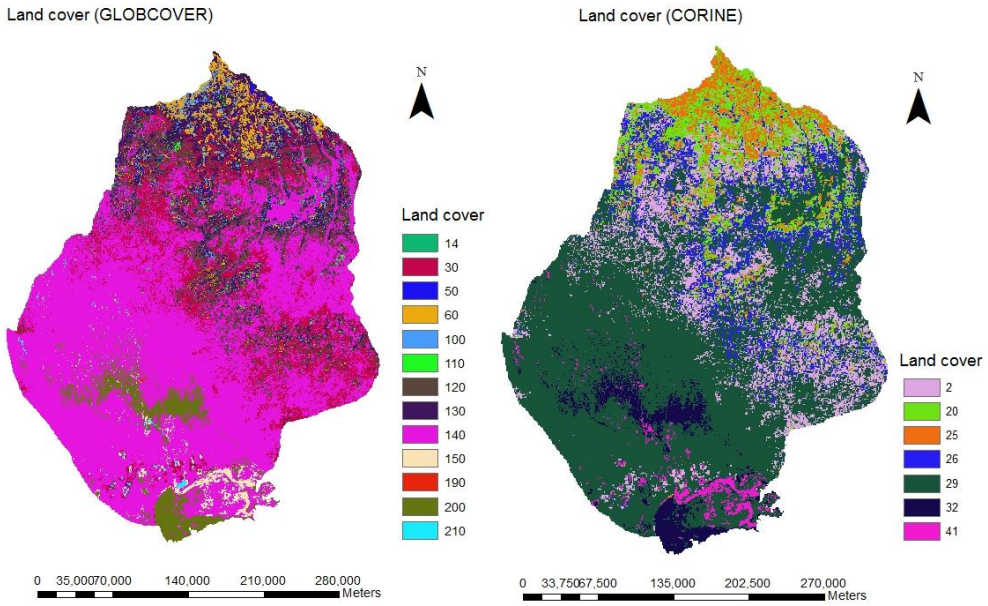

Figure 10: CORINE land cover classes and GLOBCOVER land cover classes

The Cuvelai land use polygons raster datasets was reprojected to UTM from lat-long geographic projection using the ArcMAP feature projection tool. The re-projected landuse.*shp* file was rasterized by the process of conversion from polygon to rasterin ArcMAP. The new raster dataset were resampled using nearest neighbour from the 1km spatial resolution of origin to 5km resolution [the pixel size selected for running the model]. The resampled landuse.*grid* raster data was converted from .*grid* raster to .*txt* for use in PCRaster using the ArcMAP conversion tool from raster to ascii. The new map landuse.*map* was created using the Nutshell interface of PCRaster by converting the landuse.*txt* into the final product landuse.*map* with the 'asc2map' command.

The reclassification of the land cover was based on grouping such classes as three types of forest (mixed, pine and coniferous), into one general class. The same was done for built-up areas, paved recreation areas, tarred road. This reduced the number of classes from 13 in GLOBCOVER to 6 general classes in CORINE.

4.1.4.3. Soils

The USDA taxonomy document (ftp://ftp-fc.sc.egov.usda.gov/NSSC/Soil_Taxonomy/tax.pdf) was applied to the related FAO soil order classes to obtain the values of these parameters. Water content in soils is usually expressed as either a dimensionless ratio of two masses, two volumes or is given as a ratio of a mass per unit volume as dimensionless decimal fractions or percentages, if multiplied by 100 (Lambe

and Whitman 1969). Saturated volumetric soil moisture content $(\boldsymbol{\theta_s})$ is the moisture content when all pore space is occupied by water, equivalent to porosity. Residual volumetric soil moisture content $(\boldsymbol{\theta_r})$ is remaining water at high tension (the water content for which the gradient $\boldsymbol{d\theta/dh}$ becomes zero). Pore size index $(\boldsymbol{\lambda})$ is the spaces present within a soil space and its particular soil class related to soil texture.Saturated conductivity $(\boldsymbol{K_s})$ is a measure of how conductive the soil is to the movement of water through it when it is completely filled with water. Alpha$(\boldsymbol{\alpha})$ is the Van Genuchten parameter.

The LISFLOOD model requires soil depth and soil texture to be defined for two horizons.

Table 7: Soil texture characteristics at 1m depth for LISFLOOD simulation [Horizon A]

Order	Soil texture				
	θ_s	θ_r	λ	α	K_s [cm/day]
Acrisol	0.439	0.01	0.1804	0.0314	12.061
Chernozem	0.52	0.01	0.1012	0.0367	24.8
Luvisols	0.403	0.025	0.3774	0.0383	60
Solonchacks	0.614	0.01	0.1033	0.0265	15
Solonets	0.430	0.01	0.2539	0.0083	2.272

(Source: Rawls *et, al.* 1982)

The project area was extracted from the regional soils map of Africa using the Cuvelai basin boundary Cuvelai.*shp* created in earlier steps in the ArcMAP spatial analyst tools. The vector-based soils data files were then reclassified from the FAO/UNESCO classes to match the LISFLOOD-USGS classes for which related tables are available. Soil parameters are linked to the soil texture and land use maps through look-up tables.

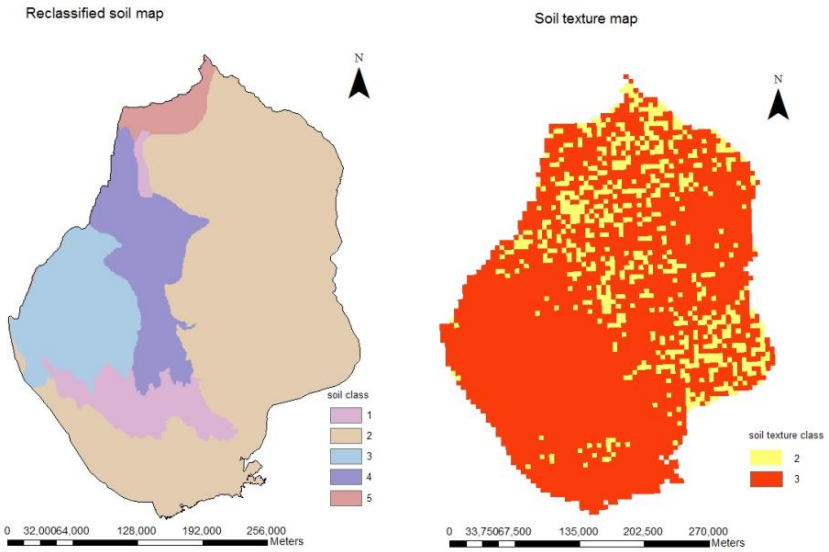

Figure 11: LIFLOOD input table for soil texture

Where code 1 is solonchacks, code 2 is solonetz, code 3 is acrisol, code 4 is chermozem and code 5 is luvisols. The soil texture map to the right is a typical PRCaster type map, where code 2 represents silt and code 3 represents clay portions of the upper soil horizon.

Table 8: LISFLOOD soil look-up tables

SOIL TEXTURE		
Table	Default name	Description
TabThetaSat1	thetas1.txt	Saturated volumetric soil moisture contentlayer 1 [-]
TabThetaSat2	thetas2.txt	Saturated volumetric soil moisture contentlayer 2 [-]
TabThetaRes1	thetar1.txt	Residual volumetric soil moisture content layer1 [-]
TabThetaRes2	thetar2.txt	Residual volumetric soil moisture content layer2 [-]
TabLambda1	lambda1.txt	Pore size index (λ) layer 1 [-]
TabLambda2	lambda2.txt	Pore size index (λ) layer 2 [-]
TabGenuAlpha1	alpha1.txt	Van Genuchten parameter α layer 1 [-]
TabGenuAlpha2	alpha2.txt	Van Genuchten parameter α layer 2 [-]
TabKSat1	ksat1.txt	Saturated conductivity layer 1 [cm day-1]
TabKSat2	ksat2.txt	Saturated conductivity layer 2 [cm day-1]

Source: van der Knijff and de Roo, 2008

The soils polygons were rasterized using ArcMAP polygon to raster conversion tool then re-projected from decimal degrees to UTM. The new soils raster datasets were resampled (nearest neighbour) from the original 300m spatial resolution to an output cell (pixel) size of 5000 meters and saved under the names soildepth and soil texture respectively for separate processing. The two soils maps were converted to *.txt* format using the raster to ascii conversion tool in ArcMAP. The '*asc2map*' command in PCRaster Nutshell was used to change the *.txt* files into useful maps soildep.*map* and soiltex.*map* that LISFLOOD will relate to associated lookup tables (**Table 8:** LISFLOOD soil look-up tables) with relevant parameters when running the code.

The soildep.*map* was created using ordinal data output format, and the soiltex.*map* was created using nominal data output format as explained in table 4 of the literature review.

asc2map *--clone* area.*map* *-N -a* soils.*txt* soiltex1.*map* (4-1)
asc2map *--clone* area.*map* *-O–a* soildepth.*txt* soildep.*map* (4-2)

4.1.4.4. Evapo-transpiration

Potential reference evapotranspiration 'ET0' is the evapotranspiration rate from a hypothetical reference vegetation with specific characteristics with unlimited availability of water (Allen *et al.*, 1998). The simulation of evaporation, water uptake and transpiration by vegetation processes in LISFLOOD involves three steps. First, potential reference evapotranspiration rate '*ET0'* is calculated. Then the potential soil evaporation rate '*ES0'* and the potential evaporation of an open water surface, *EW0*, are calculated. *ET0*, *ES0* and *EW0* are strictly climatic variables and are not influenced by any land use or soil properties. In

reality, the potential evapotranspiration can be either higher or lower than *ET0* due to differences in vegetation characteristics, aerodynamic resistance and surface reflectivity (albedo), (Allen *et al.* 1998).

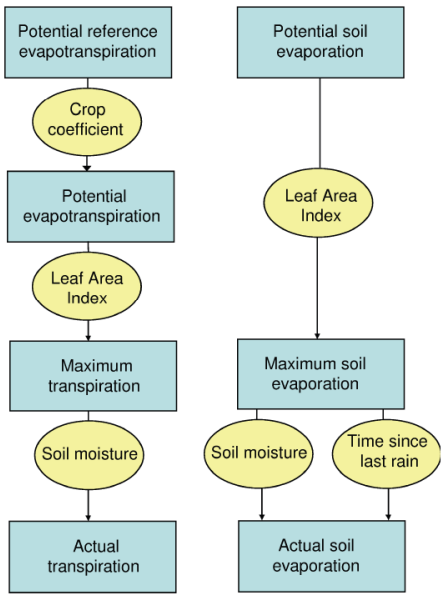

Figure 12: Main process of calculating Evapotranspiration in LISFLOOD
Source: http://floods.jrc.ec.europa.eu/files/lisflood/ec_jrc_lisvapUserManual_JvdK.pdf

The crop co-efficient was inserted as an estimate fixed value (constant raster) from literature. The LAI maps were already existent, and for the initial run, the soil moisture maps were generated by using those sourced from Outlook for Africa. The data are available at this website link: http://wxmaps.org/pix/soil10.html which avails soil moisture maps at 14 day intervals for two meters depth from the topsoil.

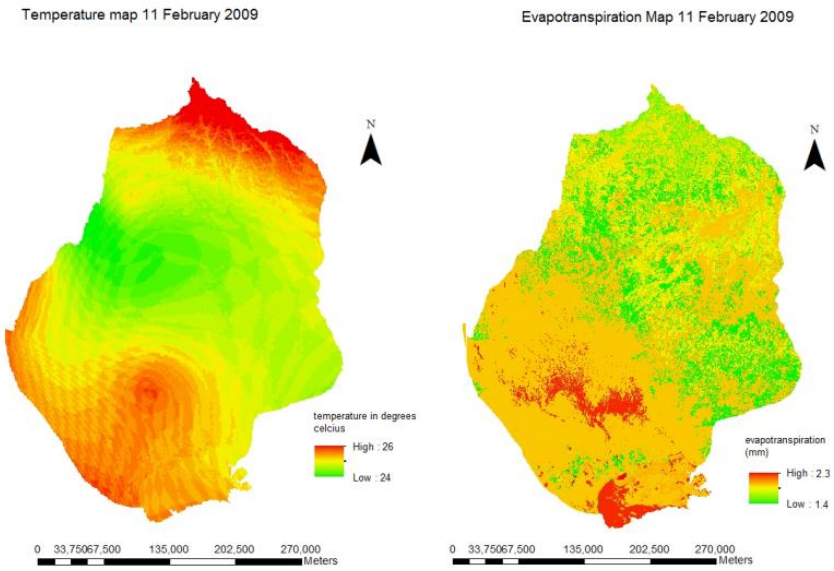

Figure 13: Visualisation of the relationship between the temperature and evapotranspiration

It can be observed that in the north of the basin, the temperatures were fairly high, but the related evapotranspiration was in the low regions. In the south of the basin, the temperatures were also high, and the evapotranspiration was fairly high. This is because the southern part is on a higher altitude and has more vegetation, so the contribution of evaporation would be less. However, in the south, at the Etosha pan, it is sparsely covered, with scattered bushes and scrubs amongst the predominant grasslands.

4.1.4.5. Land surface temperature (LST)

The decadal LST maps were read directly in ArcMAP. The area of interest was separated from the African regional data by extraction using spatial analyst tools of ArcMAP, extract by mask option. The extracted temperature maps were multiplied by a factor of 0.1 because the original data itself had been multiplied by a factor of 10. The corrected images were then resampled from 1000 meters to 5000 meters. The resampled maps were converted from *.grid* ArcMAP raster formats to *.txt* PCRaster formats. However, because the data was decadal, the numbering of the maps was respective of LISFLOOD stacking format.

Table 9: Stacking nomenclature of LST maps

Time step	Map name
1	ta000000.001
2	-
-	-
-	-
11	ta000000.011
12	-
-	-
20	-
21	ta000000.021

Source: van der Knijff and de Roo, 2008

The LISFLOOD maps were numbered according to the availability dates of the temperature stacks. However, the timesteps still run from 1 to 1000 in chronological order, and where no maps are indicated, the code uses the map of a previous timestep, until a new map is located or defined.

4.1.4.6. Precipitation TRMM v6-3B42

TheTRMM 3B42 data for the extreme rain event over Cuvelai from 21 January to 28 February 2009 were down loaded as ascii files. The ascii files were pre-processed in ILWIS using the import function with ILWIS table operator for space delimited files '*.txt*'. The data were in lat-long geographic system, so in the ILWIS import wizard, the x and y co-ordinates were defined as columns 1 and 2 respectively, with the z-value [mm] for rainfall, denoted as the third column, p. The resultant table was converted to a point map by right clicking the table in the viewer menu and using the ILWIS table operations. The point map was

then reprojected to UTM in ILWIS using the spatial reference operator. The reprojected maps were exported to ArcView Shapefile *.shp* format which is ArcGIS readable

In ArcMap the points data were interpolated to a continuous raster by inverse distance weighted (IDW) interpolation in the spatial analyst tools. The interpolation was done to output cell size 5000m, which is the equivalent of the resample raster processing option in ArcMAP data management tools. The search radius specified was variable for a 12 point consideration in the interaction options, and the interpolation was to the power 2.

The Cuvelai.*shp* boundary was used to extract the rainfall raster (product of the interpolation). The extracted map was converted to text format by using the ArcMAP raster to ascii conversion, with the prefix *'pr'*. The new rainfall text files pr001.*tx*t were converted to rainfall maps in PCRaster Nutshell using the command:

asc2map *--clone* area.*map* *-S –a*pr001.*txt*pr000000.001.*map*

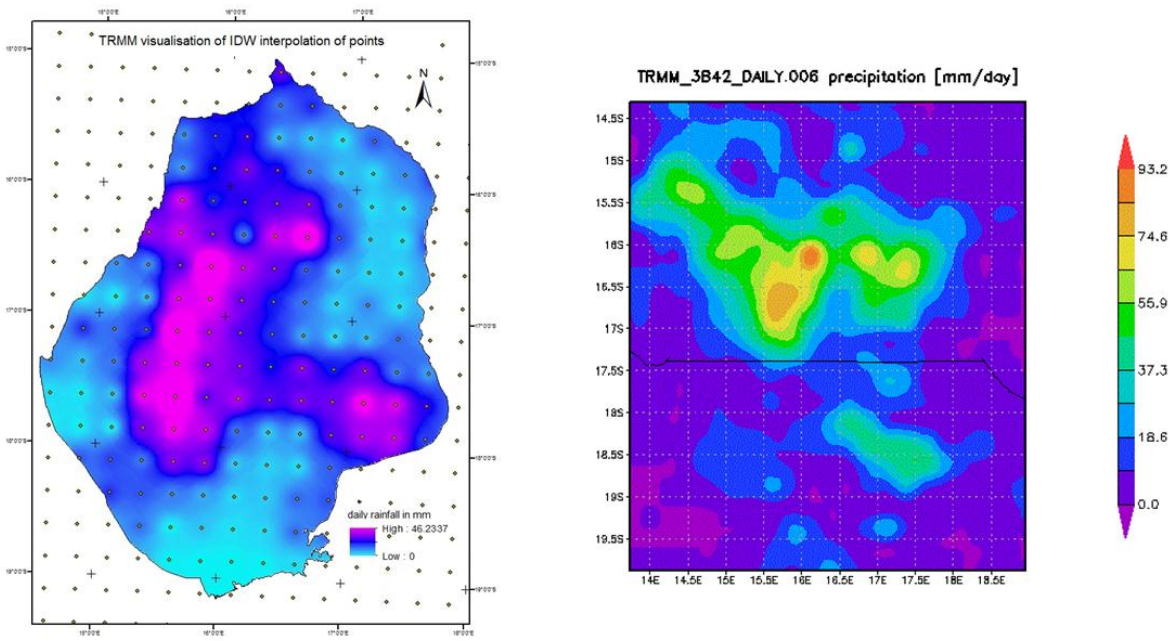

Figure 14: Demonstration of IDW interpolation of rainfall points in ArcMAP, compared with GIOVANNI TOVAS web-based visualisation

4.1.4.7. Elevation SRTM

The Cuvelai basin digital elevation model was extracted from the CGIAR-CSI (USA) server's world map by selecting grids representing the catchment area. This data is available from the following link: http://www.cgiar-csi.org/data/elevation/item/45-srtm-90m-digital-elevation-database-v41. The server has two data formats: Geotiff format for direct read in ArcMAP and ArcINFO ascii. The SRTM data are in geographic co-ordinates degrees-minutes-seconds. The multiple selection operator was used to select the grids of interest from the interactive CGIAR-CSI interface: srtm_39_17.zip , srtm_39_16.zip,

srtm_40_17.zip and srtm_40_16.zip. The four grids were unzipped and mosaicked using ERDAS imagine software. The mosaic in ERDAS was done using the MosaicPro option in the mosaic images interface available from data preparation menu under main functions.

The Cuvelai.*shp* boundary was used to extract the area of interest from the general mosaic. This new raster file was then reprojected from degrees-minutes-seconds to UTM sone 33 in the southern hemisphere. The 90m spatial resolution DEM was resampled in stages to 5000 m. The final raster, named dem.*txt* was converted to ascii format using ArcMAP, and converted to dem.map using the PCRaster asc2map command. This dem.*map* will be the used to develop other maps such as elevation range (elvrange.*map*) and local drainage direction (ldd.*map*).

4.2. LISFLOOD model setup

4.2.1. LISFLOOD model structure

The existing LISFLOOD structure requires that base maps, meteorological maps and tables are separated by storage in individual directories. All file and parameter specifications are defined in the settings file. The settingsfile has an XML structure and is made up of four elements: Ifuser, Ifoptions, Ifbinding and prolog.

Ifuser defines the paths to all input files, output files and calibration or time related main model parameters. The ifuser element is used to define (user-defined) text variables which can be used to substitute repeatedly used expressions in the binding element. In the example below, 'ifuser' always defines the path location of maps, instead of the user havingto type it in each time it is requiredby 'ifbinding'.

```
<Ifsettings>
<Ifuser>
<textvar name="PathsMaps" value="C:/LISFLOOD/MAPS">
</textvar>
</Ifuser>
<Ifoptions>
</Ifoptions>
<Ifbinding>
<textvar name="Landuse" value="$(PathMaps)/landuse.map">
</textvar>
<textvar name="SoilDepth" value="$(PathMaps)/soildep.map">
</textvar>
</Ifbinding>
</Ifsettings>
```

Ifbinding defines all the individual in and output files and model parameters. The example above shows how 'ifbinding' element provides a low level way to define all model parameter values [landuse and

SoilDepth] as well as in and output maps, time series andtables [landuse.*map* , soildep.*map*]. Individual variables are defined as 'texvar' elements within 'ifuser' / 'ifbinding'. Ifoptions switches to turn on or off specific 'options' of the model [Description after van der Knijff and de Roo, 2008].

4.2.2. Initialization of the model

The period of study is between January 21st 2010 and February 28th 2010, covering one extreme rainfall event. The model needs to have some estimate of the initial state of the internal state variables. The state of the soil at the beginning of the model run was based on satellite estimates, but this was solved by using a very long warm-up period. The meteorological and LAI maps of the study period were copied in excel using the concantenate option to replicate them for 1000 timesteps (days) which adds up to almost three years as a warm-up period.

Table 10: LISFLOOD initialisation methods

Variable	Description	Initialization method
ThetaInit1Value	initial soil moisture content upper soil layer	set to soil moisture content at field capacity
ThetaInit2Value	initial soil moisture content lower soil layer	set to soil moisture content at field capacity
LZInitValue	initial water in lower groundwater zone (mm)	set to steady-state storage
TotalCrossSectionAreaInitValue	initial cross-sectional area of water in channels	set to half of bankfull depth

Source: van der Knijff and de Roo, 2008

4.2.2.1. Initialization of the lower groundwater zone

The response of the lower ground water zone is generally very slow. A complicating factor in initialization of the lower ground water zone is that the time needed to initialise any storage component of the model is dependent on the average residence time of the water in it, (Van der Knijff and De Roo 2008). To avoid unrealistic trends in the simulations, very long warm-upperiods may be needed. LISFLOOD is capable of calculating a 'steady-state' storage amount for the lower groundwater zone. This steady state storage is very effective for reducing the lower zone's warm-up time, (Van der Knijff and De Roo 2008).The moisture content of the upper soil layer tends to respond almost instantly to LISFLOOD's meteorological forcing variables (precipitation,evapo(transpi)ration). As a result, relatively short warm-up periods are sufficient to initialise this storage component. The LISFLOOD pre-run produces a map lzavin.*map* which represents the state of the average inflow into the lower zone. This average inflow map is automatically used an input for the actual run.

4.2.3. Output generated by the model

Output is generated as either maps in PCRaster format or time series. The table below describes the output time series that are reported by default. Other outputs can be produced by activating the 'options' in –listoptions in the settings file.

Table 11: LISFLOOD default output time series (source van der Knijff and de Roo, 2008)

RATE VARIABLES AT GAUGES		
Description	**Units**	**File name**
channel discharge	m3/s	dis.tss
NUMERICAL CHECKS		
Description	**Units**	**File name**
cumulative mass balance error	m3	mbError.tss
cumulative mass balance error, expressed as mm water slice (average over catchment)	mm	mbErrorMm.tss
number of sub-steps needed for gravity-based soil moisture routine	-	steps.tss

Source: van der Knijff and de Roo, 2008

4.3. LISFLOOD rainfall-runoff modelling

The equations involved in creating the LISFLOOD input parameter maps have been provided in Appendix 4 Lisflood parameter derivation equations.

4.3.1. Simulation and reporting of water levels

Within LISFLOOD it was possible to simulate and report water levels in the Cuvelai basin channel. This was done by activating the 'simulateWaterLevels' option in the 'Ifoptions' element of the settings file:

<setoption name="simulateWaterLevels" choice="1" />

This enables the calculation of water levels for the channel pixels using kinematic wave routing. The reporting (production) of water level maps (interpreted as inundation maps) is activated using the option:

<setoption name="repWaterLevelMaps" choice"1" />

It is important to note that the repWaterLevelMaps means the LISFLOOD model should 'report' or 'produce' an output and the choice is default value zero for report no maps, so this is changed to one for produce map(s). The reporting options are only effective if the 'simulateWaterLevels' option has been activated by changing the choice value from default zero to one. In both cases the choices are exclusively

either zero or one no other number will activate this option. The channel bottom width map 'chanbw.*map'* and the channel bankful maps 'chanbnkf.*map'* respectively are critical to the accurate simulation of the calculation of water levels.

4.3.2. Calculation of water levels

LISFLOOD by default uses the kinematic wave routing for calculation of water levels for channel pixels within any given catchment. LISFLOOD has the option to implement the dynamic wave routing, however for this study, the default kinematic routing was used (**Figure 15:** Kinematic wave routing (Source van der Knijff and de Roo, 2008)). The option to use the dynamic wave is applicable only if the researcher has access to additional required data such as channel cross section information, wetted perimeter and sequence of water levels.

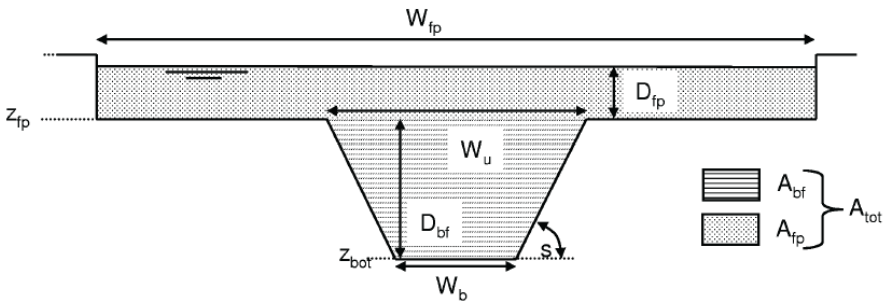

Geometry of channel cross-section in kinematic wave routing. W_b: channel bottom width; W_u: channel upper width; z_{bot}: channel bottom level; z_{fp}: floodplain bottom level; s: channel side slope; W_{fp}: floodplain width; A_{bf}: channel cross-sectional area at bankfull; A_{fp}: floodplain cross-sectional area; D_{bf}: bankfull channel depth, D_{fp}: depth of water on the floodplain

Figure 15: Kinematic wave routing (Source van der Knijff and de Roo, 2008)

The water levels calculated using the kinematic wave routing are relative to the channel bottom level (z_{bot}), (van der Knijff and de Roo, 2008). The water levels flow directly from the channel bottom width, sideslope and bankfull level. The channel bottom level is defined in LISFLOOD as '*chanbw.map'*. The channel bankfull level is defined in LISFLOOD as '*chanbnkf.map'*. When the channel bottom width exceeds the bankfull cross sectional area, the surplus will be evenly distributed over the flood plain. The depth of water on the flood plain is then added to the bankful channel depth. In order to calculate the water levels, LISFLOOD needs a map of flood plain width which is defined in the 'ifbinding' variable 'FloodPlanWidth'. It is given the default name '*chanflpn.map'*.

4.4. LISFLOOD calibration

Traditionally hydrological models are considered as difficult to calibrate.The manual calibration of distributed hydrological models is often costly on computation, thus restricting the feasible number of model runs. The calibration was run for a period of 6 months as warm up (183 days) for initialisation of

LISFLOOD for the Cuvelai basin. The present LISFLOOD version contains 24 process-related parameters, (van der Knijff *et al.,* 2008) are all of which are defined in the 'lfuser' element, and default values are given for each of them. Using the guidance from the LISFLOOD manual, the following internal state variables were set to zero at the start of the run:

WaterDepthInitValue	amount of water on the soil surface,
FrostIndexInitValue	frost index
SnowCoverInitValue	snow cover
CumIntInitValue)	interception storage,
UZInitValue	storage in the upper groundwater zone.

The initial value of the days since last rainfall event (*DSLRInitValue*) was set to 1. The amount of water in the channel (defined by *TotalCrossSectionAreaInitValue*) is highly spatially variable (limited by the channel geometry). The amount of water that can be stored in the upper and lower soil layers (*ThetaInit1Value*, *ThetaInit2Value*) is limited by the soil's porosity. LISFLOOD provides the possibility to initialise these variables internally, and these special initialisation methods can be activated by setting the initial values of each of these variables to a special 'bogus' value of *-9999*.

The two infiltration parameters *b_Xinanjiang* (b) and *PowerPrefFlow* (c_{pref}) are empirical parameters that are treated as calibration constants in the LISFLOOD model.

$$A_s = 1 - (1 - {}^{W_1}/_{W_{s1}})^b \quad (5\text{-}1)$$

Where:

A_s	saturated storage fraction of soil
${}^{W_1}/_{W_{s1}}$	maximum and actual amounts of water in the upper soil layer respectively

$$D_{pref,gw} = W_{av}({}^{W_1}/_{W_{s1}})^{c_{pref}} \quad (5\text{-}2)$$

Where:

W_{av}	amount of water available for infiltration
$D_{pref,gw}$	amount of preferential flow per timestep [mm]

The groundwater parameters are also treated as calibration constants, except *GwLossFraction* which is kept at zero, unless deep groundwater systems exist or else prior information indicates that groundwater is lost beyond the catchment boundaries. This leaves U*pperZoneTimeConstant , LowerZoneTimeConstant* and *GwPercValues* as the calibration constants. Where:

GwLossFraction(f_{loss})	rate of flow out of the lower groundwater zone, expressed as a fraction of the total outflow
UpperZoneTimeConstant(T_{uz})	time constant for the upper groundwater zone [days]
LowerZoneTimeConstant(T_{lz})	time constant for the lower zone in days
GwPercValues (GW_{perc})	the maximum rate of percolation going from the upper to lower groundwater zone (mm/day)

4.5. LISFLOOD Flood mapping

LISFLOOD has a variety of output options for flood mapping available as either maps or timeseries format. Output files can be turned on or off using options in the LISFLOOD settingsfile. All options by default are set to zero, and the user can identify the options relevant to the objectives of the study on a needs basis.

4.5.1. Flood mapping

The PCRaster flood maps were exported into ArcGIS raster formats. The raster maps were converted into polygons using the ArcMAP data conversion toolbox function. Using a new boundary based on the existing flood maps from the TERRA SAR images, the inundation polygons were overlaid on the digital elevation level map, with the rivers layer to show the position and extent of inundation related to the elevation. The flood maps are available at the following websites: http://www.zki.dlr.de/map/214 for the February- March 2009 floods and http://www.unitar.org/unosat/node/44/1168 for the March - April floods. The Terra SAR flood rasters are available at the following link: http://www.zki.dlr.de/article/843

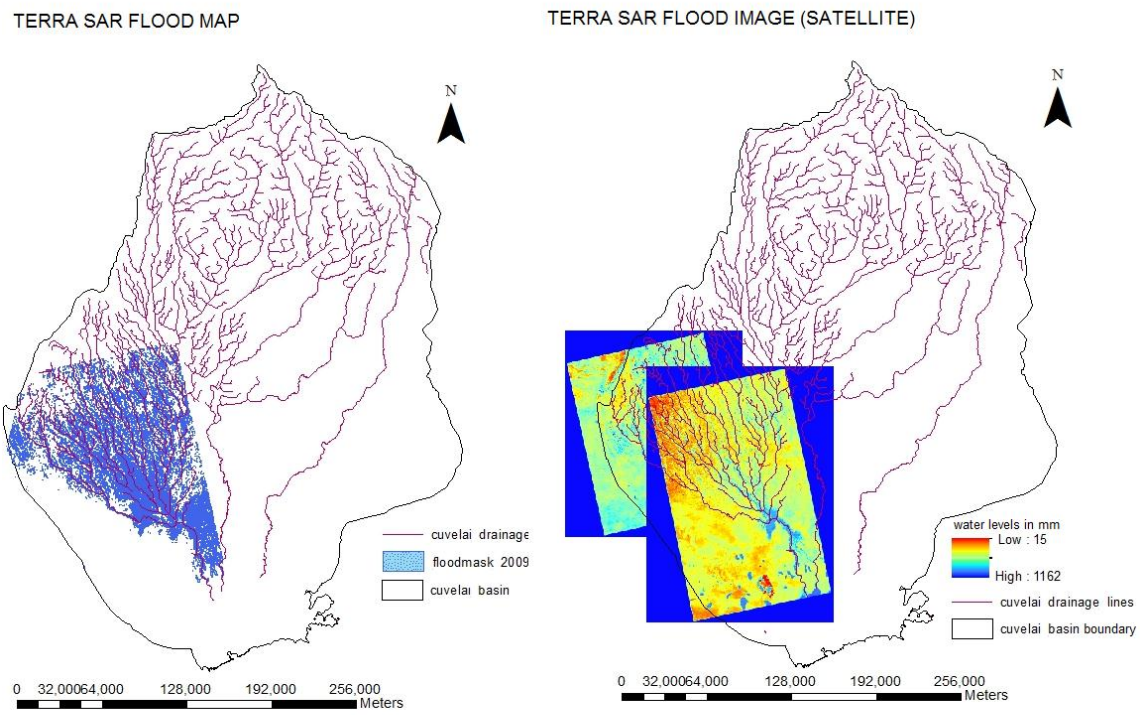

Figure 16: Visualisation of the Terra Sar flood mapping efforts (21 March 2008)

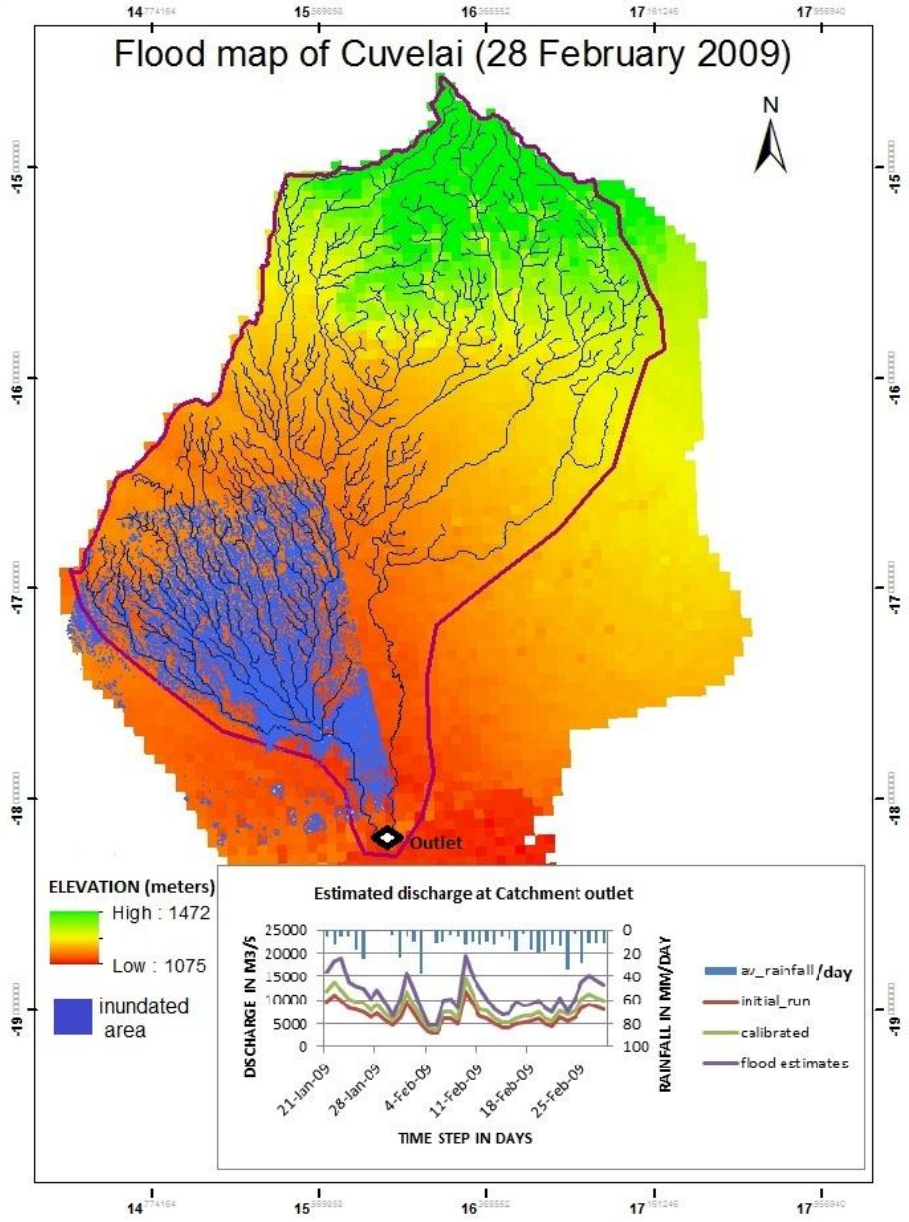

Figure 17: LIFLOOD inundation map for last timestep 28 February 2009

4.6. Objective functions

4.6.1. The Root Mean Squared Error (RMSE)

The root mean squared error is not standardized, but is expressed in terms of the original variables. This makes it difficult to look at it on its own when assessing model performance. To get a feel for the

magnitude of the RMSE it can be compared with the mean of the absolute prediction error (forecast - actual). The closer RMSE is to the mean the better the performance of the model.
The formula for RMSE reads:

$$RMSE = [\frac{1}{n}\sum_{i-1}^{n}(Q_{measured} - Q_{calculated})_i^2]^{0.5} \quad (5\text{-}3)$$

Where:
$Q_{measured}$ is the measured discharge before calibration
$Q_{calculated}$ is the modeled discharge after calibration

The differences between the initial forecasts and the corresponding post-calibration observed values are squared and then averaged over the sample, and the root is taken. Since the errors are squared before they are averaged, the RMSE gives a relatively high weight to large errors. This is most useful when large errors are particularly undesirable.

4.6.2. The Nash-Sutcliffe coefficient of efficiency (NS)

The Nash–Sutcliffe coefficient is used to assess the model efficiency hydrological models.

$$NS = 1 - \frac{\sum_{n=1}^{N}(Q_o^n - Q_m^n)^2}{\sum_{n=1}^{N}(Q_o^n - \bar{Q}_o)^2} \quad (5\text{-}4)$$

Where:
Q_o is observed discharge
Q_m is modeled discharge
($\bar{Q}_o$) is the mean value of the observed discharge

A value of 1 indicates a perfect agreement between observed and simulated discharge. When <0 it indicates that the mean of the observations is a better predictor than the simulated values. Negative values indicate that the observed mean discharge is a better predictor than the model simulated discharge. Values between 0.9 and 1 indicate that the model performs extremely well and performance decreases as values decrease. Values between 0.6 and 0.8 indicate that the model performs reasonably well.

4.6.3. Cumulative Mass Balance Error

Mass balance errors are displayed in the post-processor output files of LISFLOOD to give an indication of the accuracy with which the water balance equations are being solved. Mass balance error alone, however, may not be a valid indicator of simulation accuracy. A small mass balance error may not indicate a high degree of accuracy, but a large mass balance error is usually indicative of low accuracy. An error of 0% would indicate that mass is being perfectly conserved. It is desirable to have the total simulation mass balance error less than about 1%. Errors greater than this may indicate failure to reach the desired level of accuracy. There can be a discrepancy on the very first time step of a simulation when there is an inconsistency between initial and boundary conditions resulting in a situation situations when a relatively

large mass balance error may not be indicative of solution error. This occurs when changing constant head boundaries for a recharge period.

5. RESULTS AND ANALYSIS

In this study, the flood maps of February-March 2009 are considered to be the true discharge data. The model was initialised using a timestep of 1000 days, then the period of 40 days was isolated for the analysis, from 21 January to 28 February.

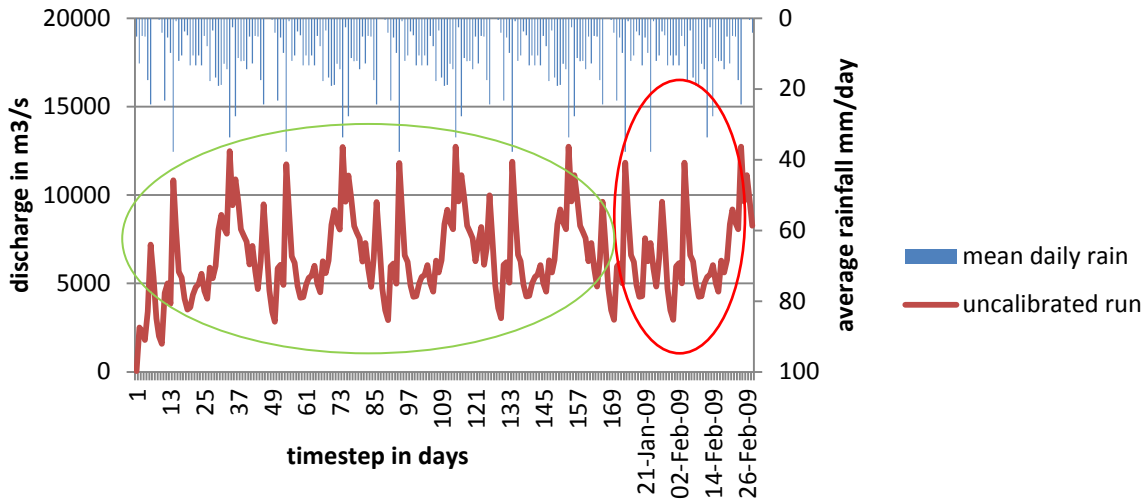

Figure 18: Plot of model simulated discharge against rainfall received

It can be observed that the peaks of the discharge from the period of interest marked in the red circle, was not entirely corresponding to the rainfall received. Thus a calibration of the model was carried out to improve the 'coincidence' of the peak flows with the maximum average daily rainfall received. This was done by conducting sensitivity analyses for five parameters suggested by van der Knijff and de Roo (2008). These parameters are: two infiltration parameters *b_Xinanjiang* (b) and *PowerPrefFlow* (c_{pref}) as well as *UpperZoneTimeConstant* (T_{uz}), time constant for the upper groundwater zone [days]; *LowerZoneTimeConstant* (T_{lz}), time constant for the lower zone in days and *GwPercValues* (GW_{perc}), the maximum rate of percolation going from the upper to lower groundwater zone (mm/day)

5.1. Sensitivity analysis results

5.1.1. Response of the UZTC

The chart overleaf indicates the response of the ascending and descending limb to changes in upper zone time constant. This is clearly visible in the periods between 2 and 8 February as well as round 25-28 February. The model has low sensitivity to the UZTC. This is observed in the similar trend of the lines in terms of the shape of the hydrograph, as well as no major differences in discharge between the extreme UZTC parameters of of 5 and 45 respectively.

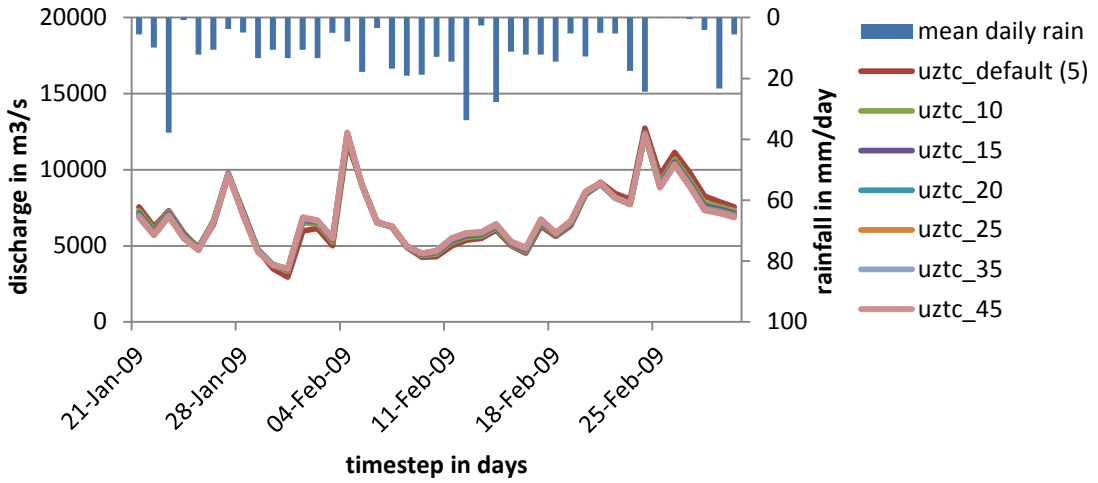

Figure 19: Sensitivity of the model to change in UZTC

There is not much influence of the UZTC on the positioning of the peaks in relation to the rainfall received because it primarily affects the residence time (in days) in the upper groundwater zone. However, it is observed that the UZTC influences the receeding limb of the hydrograph noticeably on the periods 30 January to 3 February and 11 to 17 February following consistently high rain events above 10mm/day each. An anomally occurs at the period 25 to 28 February with an unexpecte rise in dicharge following one day with very little rainfall less than 2mm/day on average.

5.1.2. Response of the LZTC

The lower zone time constant the residence time in the lower ground water zone. It controls the amount and timing of outflow from the ground water resevoir which reflects in the river bank as discharge. Figure 12 shows the sensitivity of the LZTC according to the tests carried out.

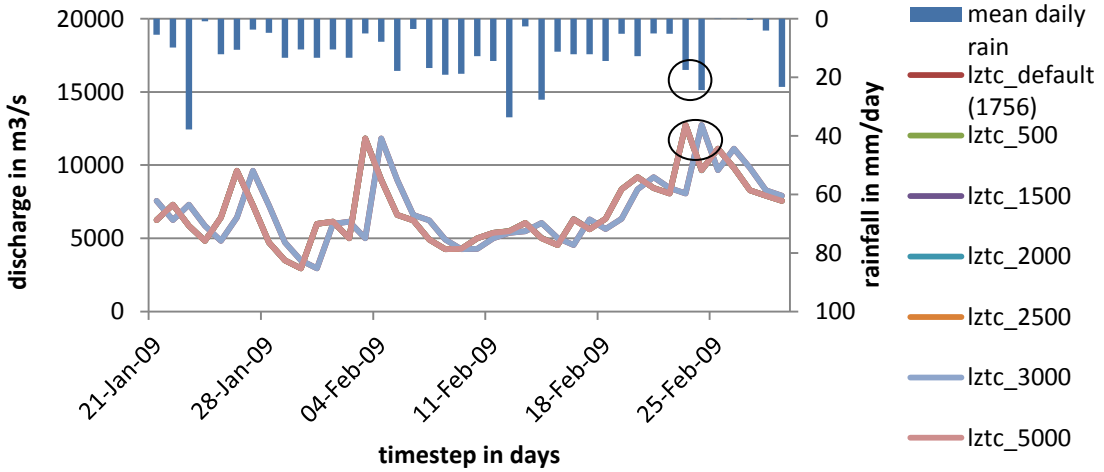

Figure 20: Sensitivity analysis of LZTC

There is a more pronounced sensitivity of the LZTC than the UZTC to the peak flows.The increase in LZTC values shifts the peak flows to coincide more with the average daily rainfall, as can be seen with the change on 23 to 25 February marked with a black circle.

5.1.3. Response of GWPercValue

The ground water percolation values controls the flow from the upper to the lower ground water zone. Increasing the value of GPV decreases the amount of water available as base flow by very small valuesas indicated in the figure below.The low value of GPV_0 yields higher peaks than GPV_1.2 and GPV_1 respectively.The discharge generated does not have a very big margin, so it appears the GPV parameter has low sensitivity.

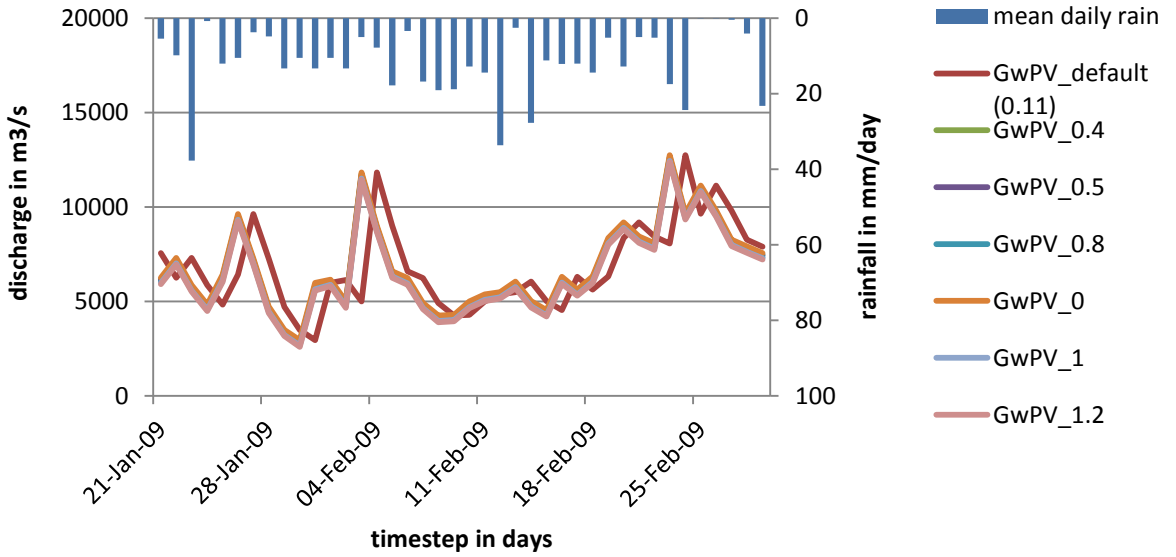

Figure 21: GPV sensitivity analysis

5.1.4. Response of b_X parameter

Increasing the value of b_X affects simulation of infiltration. The b_X parameter controls the fraction of saturated area within a grid cell that is contributing to runoff, thus it is inversely related to infiltration. It is expected that high b_X values would decrease the infiltration, and ultimately increase surface runoff (quick-flow).

The general observation is that the model is very sensitive to the changes in the b_X parameter values. The role of b_X as a shape parameter is seen in figure 12 below where the ascending and descending limbs are visibly different for b_X values of 0.1 and 0.2 which develop gentle receeding limbs for the periods (7 to 13 February; 19 to 21 February and 24 to 28 February). The higher b_X parameter values of 0.8 and 1 maintain the shape of the hydrograph, while the b_X value of 0.5 is inbetween the two extremes.

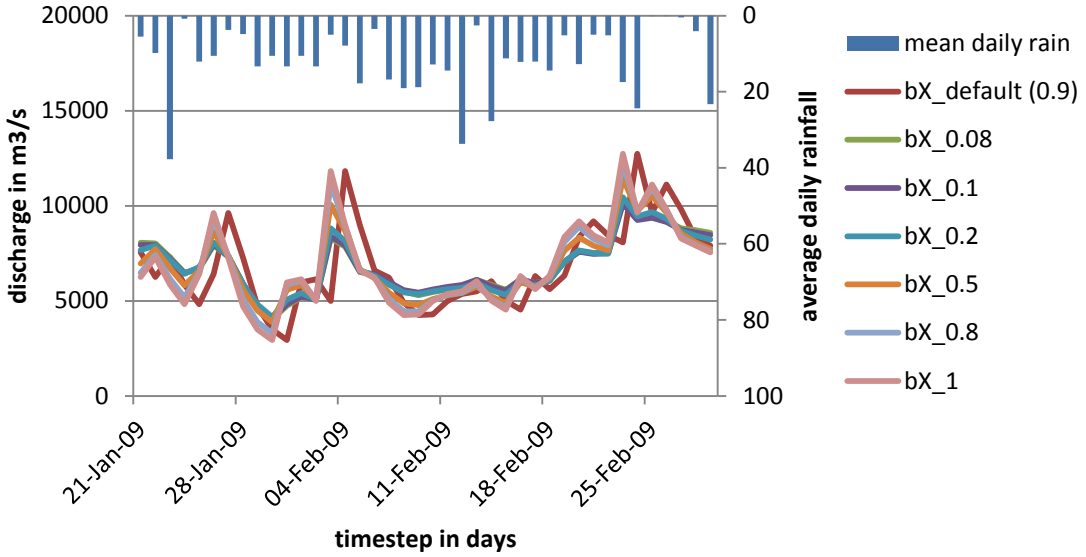

Figure 22: Sensitivity analysis on the b_X parameter

5.1.5. Response of PPF parameter

The power preferential bypass flow parameter is an empirical shape parameter. It relates the preferential flow to soil saturation. For this study, the soil is already saturated, since the days since last rainfall event is zero and ultimately, the process of flooding had already begun in some parts of the catchment. This affected the sensitivity of the PPF, as seen in the chart below. The peak flows are maximum at PPF value of 6, however, this significantly slowed down the speed of processing. Therefore based on a comparison of the overall model performance and objective functions (root mean squared error and Nash Sutcliffe), the value 5 was selected instead.

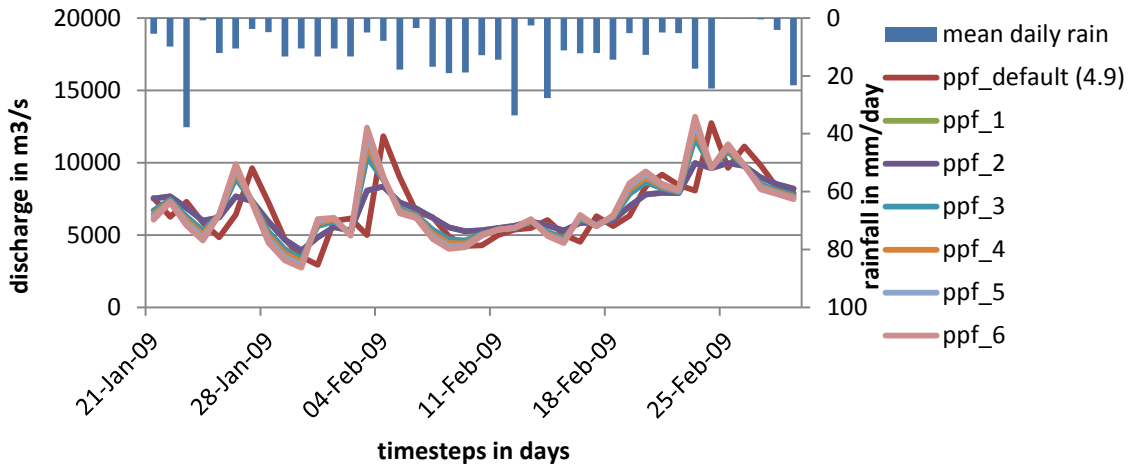

Figure 23: Sensitivity analysis for PPF parameter

The following table shows the results of the sensitivity analysis carried out. The figures highlighted are the optimal based on the calibration against the occurrence of rainfall peaks in relation to observed discharge.

Table 12: Results of the sensitivity analysis carried out on LISFLOOD calibration parameters

	RUN	PARAMETERS					OBJECTIVE FUNCTIONS	
		UZTC	LZTC	GPV	bX	PPF	RMSE	NS
Upper Zone	**default**	5	1756	0.11	0.9993	4.9043	89.60	0.57
	2	10	1756	0.11	0.9993	4.9043	91.70	0.55
	3	**15**	**1756**	**0.11**	**0.9993**	**4.9043**	**90.33**	**0.58**
	4	20	1756	0.11	0.9993	4.9043	90.69	0.56
	5	25	1756	0.11	0.9993	4.9043	89.75	0.57
	6	35	1756	0.11	0.9993	4.9043	89.42	0.57
	7	45	1756	0.11	0.9993	4.9043	89.21	0.57
Lower Zone	**default**	5	1756	0.11	0.9993	4.9043	90.57	0.56
	2	5	1500	0.11	0.9993	4.9043	81.75	0.55
	3	5	500	0.11	0.9993	4.9043	91.43	0.53
	4	5	2000	0.11	0.9993	4.9043	88.05	0.58
	5	**5**	**2500**	**0.11**	**0.9993**	**4.9043**	**91.19**	**0.59**
	6	5	3000	0.11	0.9993	4.9043	87.14	0.59
	7	5	5000	0.11	0.9993	4.9043	88.19	0.58
GwPercValue	**default**	5	1756	0.11	0.9993	4.9043	84.01	0.61
	2	5	1756	0	0.9993	4.9043	82.63	0.63
	3	5	1756	0.4	0.9993	4.9043	83.28	0.63
	4	5	1756	0.5	0.9993	4.9043	84.19	0.61
	5	5	1756	0.8	0.9993	4.9043	83.94	0.62
	6	5	1756	1	0.9993	4.9043	82.62	0.63
	7	**5**	**1756**	**1.2**	**0.9993**	**4.9043**	**84.94**	**0.62**
b_Xinanjiang	**default**	5	1756	0.11	0.9993	4.9043	92.63	0.52
	2	5	1756	0.11	0.08	4.9043	91.30	0.55
	3	5	1756	0.11	0.1	4.9043	88.05	0.58
	4	5	1756	0.11	0.2	4.9043	87.19	0.59
	5	5	1756	0.11	0.5	4.9043	89.75	0.57
	6	**5**	**1756**	**0.11**	**0.8**	**4.9043**	**92.43**	**0.60**
	7	5	1756	0.11	1	4.9043	90.76	0.60
PowerPrefFlow	**default**	5	1756	0.11	0.9993	4.9043	94.63	0.52
	2	5	1756	0.11	0.9993	1	82.63	0.63
	3	5	1756	0.11	0.9993	2	83.28	0.63
	4	5	1756	0.11	0.9993	3	91.49	0.55
	5	5	1756	0.11	0.9993	4	83.01	0.63
	6	**5**	**1756**	**0.11**	**0.9993**	**5**	**91.30**	**0.63**
	7	5	1756	0.11	0.9993	6	90.16	0.56

The optimum values have been determined for the Cuvelai basin LISFLOOD run as follows:

Table 13: Summary of final otimised values against upper and lower bounds

	Parameters				
	UZTC	LZTC	GPV	bX	PPF
Range[1]	1 – 50	50 – 5000	0 – 1.5	0.1 - 1	1 – 6
Range[2]	1 - 10	10 – 5000	0 - 0.5	0.05-0.5	5-15
Default	5	1756	0.11	0.993	4.9043
Optimum	15	2500	1.2	0.8	5

Source : range[1]and default values: (van der Knijff and de Roo, 2008) range[2] : (Feyen , 2005)

5.1.6. Validation of the model

Previous flood maps were converted to point maps then the points were interpolated to produce a total coverage of the study area. The new maps were run through the same process as the original TRMM data to generate PCRaster rainfall maps as textfiles in ArcMAP, that could be used to run the model (when converted to *.map* format) and validate the model's performance after the callibration. The integrity of the flood maps is not guaranteed, as they were sourced in different formats and from independent sources from the internet. Detailed information on the flood maps is available on the following links:
http://sensorweb.nasa.gov/Gallery.html ;
http://earthobservatory.nasa.gov/NaturalHazards/view.php?id=37736 ;
http://www.unitar.org/unosat/node/44/1168

The flood maps of 2009 were used as the actual 'observed' discharge and the two runs were used as the simulated discharge. The following are the results for the two objective functions.

Table 14 : RMSE and Nashsutcliff test for pre-calibration and post-calibration runs against the flood maps

Model run	RMSE	Nash Sutcliffe
Precalibration	82.63	0.63
Post-calibration	83.28	0.59

The figure bbelow confirms the outcome of the objective functions. As the calibrated run appears to have a similar shape na doutput as compared with the actual discharge based on the flood maps in figure 17 overleaf.

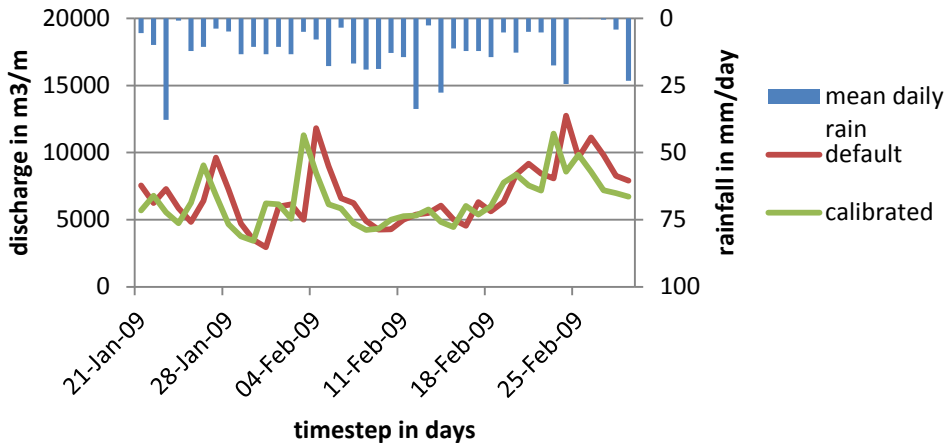

Figure 24: Comparison of the post-calibration and pre-calibration discharges

There has been displacement of the peak discharges and to an extent an increase in the baseflow between 26 January and 10 February 2009 as a result of the calibration of LISFLOOD in the context of this study. This would be ideal as previous studies have indicated that at large spatial resolution, the accuracy of rainfall measurement from space using remotely sensed images can be highly inaccurate and give an underestimate of the actual conditions on the ground.

Figure 25: Validation of model performancebelow shows the behaviour of the three different discharge simulations resulting from the study. It can be observed that neither the post-calibration nor the pre-calibration runs with theTRMM data accurately define the shape of the hydrograph with reference to discharge inferred from previous flood maps. However the calibrated discharge shows a better estimate ofdischarge compared to the pre-calibration discharge. The relationship between the flood maps and the rainfall remains doubtful, as some of the peaks do not correspond to the rainfall events observed at the time.

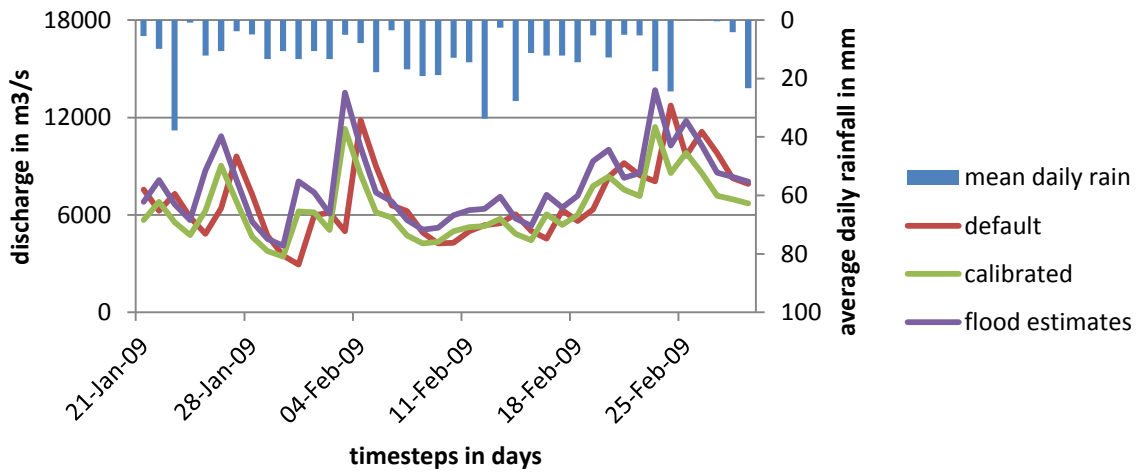

Figure 25: Validation of model performance

A comparison of the cummulative mass balance error generated by the model for the pre-calibration and the post-calibration discharges generated are shown below. It can be observed that the error is significantly reduced from close to 0.008 in the pre-calibration discharge to almost 0.005 after calibration at endtime (timestep 1000). The mass balance error on its own is not a reliable indicator of the accuracy of LISFLOOD in simulating discharge, however, coupled with other best practices such as the two objective functions RMSE and Nash Sutcliie, reasonable decuctions on model performance can be made.

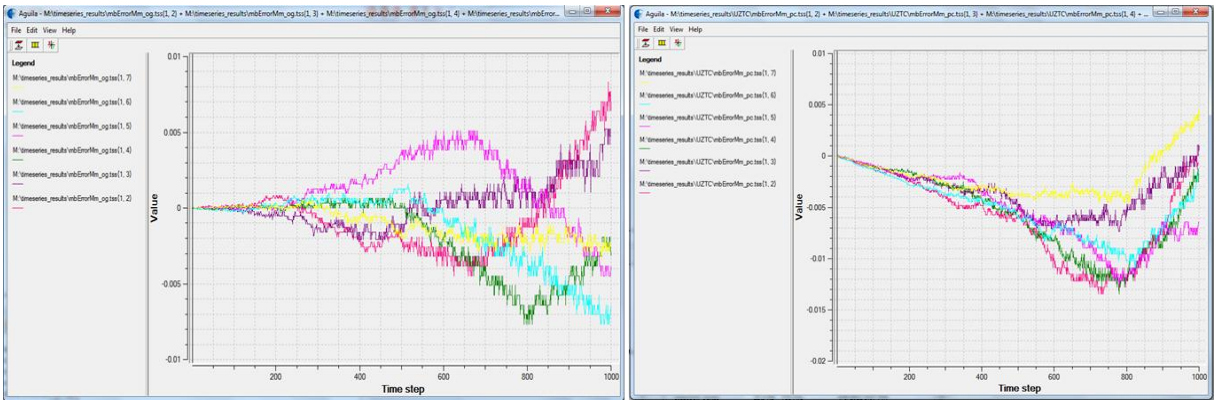

Figure 26: Cummulative mass balance error before calibration and cummulative mass balance error after calibration

Inundations maps were produced for the smaller portion of the Cuvelai basin for which validation data was available. It can be observed from the figure below that mainly the low elevation areas in the south-west were flooded. The Cunene sub-basin had full coverage of satellite imagery compared to the rest of the catchment, marked by the maroon boundary. This is an area of interest because it is an area of high agriculture activity and over 75% of Namibia's rural population resides here.

6. CONCLUSIONS AND RECOMMENDATIONS

6.1. Conclusions

The general conclusion is that it is possible to simulate flood events based on short term extreme rainfall events for –non-European catchments using LISFLOOD. However the simultaion of the model could be improved with much more accurate and basin specific data.

The analysis showed that the model is very sensitive to the parameters b_X and PPF along the ascending and receeding limbs of the hydrographs. This would be expected as both are empirical shape parameters, with bX simulating infiltration and PPF relating preferential flow with soil saturation. The GPV and LZTC both control slow runoff mechanisms and are more sensitive to the 'timing' of the peaks and show a shift towards better coincidence with rainfall events. The UZTC is the least sensitive of the parameters, and generally any values within the suggested range can be used within the context of this study and with the dataset available because from a minimum of 10 to a maximum of 50 the response is almost negligible.

The channel bottom width map 'chanbw.map' and the channel bankful maps 'chanbnkf.map' respectively are critical to the accurate simulation of the calculation of water levels through kinematic routing. General assumptions were used for these maps and this could have affected the overalll discharge simulated as seen in figure 25, that the calibrated run produced much lower discharge compared to the discharged generated by the 'previous' flood maps.

Insufficient validation data was available both spatially and temporally. There was data for only one day overlapping the simulation period, which was 28 February 2009. Therefore outside of extracting only the area of interest, no other gain could be made of this single dataset for either accurate calibration or validation.

A duplicate dataset for the LISFLOOD run had been developed at an earlier stage of the study at higher spatial resolution of 1 kilometer, compared with the current coarse resolution of 5 kilometers. However, many computational errors were encountered. It still stands to be investigated whether the LISFLOOD runtime errors were as a result of the computational burden of a finer scale model, or a simple matter of erraneous data possibly containing some missing values.

6.2. Recommendations

The flexibility of LISFLOOD regarding the selection of its calibration parameters poses the risk of over parameterisation, (van der Knijff and de Roo, 2008). This is because in the absence of sufficient prior data of good quality, other parameters can be included in the calibration process. Since constant values were

used for the calibration of LISFLOOD in the Cuvelai case study, it is recommended to define each calibration parameter as a spatially distributed grid by replacing the single values with representative heterogenous maps. This would account for within basin variability within the basin, rather than a single value estimation which suggests homogeneity.

According to van der Kniff and de Roo (2008) all water levels are relative to channel bottom level. Therefore the channel bottom width map 'chanbw.map' and the channel bankful maps 'chanbnkf.map' respectively are critical to the accurate simulation of the calculation of water levels in generation of inundation maps using the kinematic wave. The figures used in the study for both maps were estimates.It could be beneficial to conduct a thorough study of the channels and get the correct channel dimensions to put into the LISFLOOD model.

There is also need for consistent ground truth rainfall data such that the validationn of the model can be more effective. The little data available for validation of the model could also lead to inaccurate assessment of the overall performance of the model as was the case, where there was a smaller coverage of 'flood maps' used in the validation compared to the actual size of the catchment of interest.

Where possible , automated calibration is recommended, as the manual calibration is subject to human error, since it is a cumbersome task to go through every possible value within the suggested upper and lower bounds of the range of values for the calibration parameters. To overcome the computational burden of manual calibration, automated methods could be used for further, detailed study of the hydrological response of the Cuvelai basin to extreme rain events on a short time period.

TRMM-3b-42 has a 3 hourly rainfall product which can be used to substitute the daily rainfall product used in the study. This could improve the model simulation of discharge as well, if the daily rainfall is replaced by three hourly rainfall for a short time frame like that of 40 days used in the study.

In studies where flood events are simulated, an overestimation can be a better error than an underestimation which could affect early warning systems, thus causing loss of human and animal lives, and extensive socio-economic damage. A great benefit could be expected from the introductionof a finer calibrated model into the forecasting system to better capture the magnitudeand the timing of floods. For detailed study of flood patterns in the Cuvelai basin, it would be recommended that a proper and detailed calibration be carried out to improve the performance of the model and assist in decision making and understanding of the catchment response to extreme rainfall events.

LIST OF REFERENCES

Allen, R. G., Pereira, L. S., Raes, D. and Smith, D. (1998) Crop evapotranspiration - guidelines for computing crop water requirements. 56 — FAO Irrigation and Drainage Papers

Barnard, P. (1998). "Biological diversity in Namibia" Windhoek, Namibia: Namibian National Biodiversity Task Force.

Baret, F., O. Hagolle, B. Geiger, P. Bicheron, B. Miras, M. Huc, B. Berthelot, f. Nino, M. Weiss, O. Samain, J.L. Roujean, and M. Leroy, LAI, FAPAR, and FCover CYCLOPES global products derived from Vegetation. Part 1: principles of the algorithm, Remote Sensing of Environment, 110:305-316, 2007.

Bittner Water Consultant (BIWAC) (2004).Demarcation of Water Basins on National Level.Study on behalf of Deutsche GesellschaftfürTechnischeZusammenarbeit (GTZ).Windhoek

Central Bureau of Statistics (2003) 2001 Population Housing and Census.NationalReport.Basic Analysis with Results.Windhoek

Contreras, S., Boer, M. M., Alcalá, F. J., Domingo, F., García, M., Pulido-Bosch, A., et al. (2008). An ecohydrological modelling approach for assessing long-term recharge rates in semiarid karstic landscapes. [doi: DOI: 10.1016/j.jhydrol.2007.11.039]. *Journal of Hydrology, 351*(1-2), 42-57.

Commission of the European Communities (CEC) (1993) CORINE Land Cover, Guide Technique. Office for Publications of the European Communities , Luxemburg — EUR 12585EN

Duan, Q. Gupta, V. & Sorooshian, S., 1993, Shuffled complex evolution approach for effective and efficient global minimization, J Optim Theory Appl, Kluwer Academic Publishers-Plenum Publishers, 76, 501-521

De Roo, A.P.J. (2010). LISFLOOD Distributed Water Balance and Flood Simulation Model. Setting up the model.

De Roo, A. P. J. , Wesseling, C. G. and Van Deursen, W. P. A. (2000) Physically based river basin modelling within a GIS: The LISFLOOD model.. Hydrological Processes 14 , pp. 1981-1992.

De Roo, A.P.J., L. Hazelhoff and P.A. Burrough 1989. 'Soil erosion modelling using 'ANSWERS' and Geographical Information Systems'. Earth Surface Processes and Landforms, 14, 517-532.

De Roo, A.P.J., C.G. Wesseling & C.J. Ritsema 1996. 'LISEM: a single event physically-based hydrologic and soil erosion model for drainage basins. I: Theory, input and output'. Hydrological Processes, 10-8, 1107-1117.

De Roo, A.P.J. 1996 'Soil Erosion Assessment Using GIS.' In: Singh, V.P. and Fiorentino, M. (eds.) Geographical Information Systems in Hydrology. Kluwer. 443 p.

DWAF (2010). "Rural water developing and planning." Retrieved 17 August 2010, from http://www.mawf.gov.na/Directorates/RuralWaterSupply/support.html.

DWAF, 2008 http://www.nnf.org.na/ENVDIR/index.htm

El Bastawesy, M., White, K., & Nasr, A. (2009). Integration of remote sensing and GIS for modelling flash floods in Wadi Hudain catchment, Egypt. *Hydrological Processes, 23*(9), 1359-1368.

EUMETSAT (1996).Meteorological Products Extraction Facility (MPEF).Algorithms Specification Document, EUMETSAT.Doc.No.MTP.SPE030.

Fairfield, J., & Leymarie, P. (2009). Drainage networks from grid digital elevation models. *Water Resour. Res., 27*(5), 709-717.

FAO (1998).World Reference Base for Soil Resources. Rome, FAO.

FAO/UNESCO (1974) Soil map of the world, 1:5 000 000, ten volumes, Unesco-Paris

Farr, T., G and M. Kobrick (2000).The Shuttle Radar Topography Mapper.NASACenter. J. P. Laboratory. USA. 200 10012851.

Feyen, L. (2005) Calibration of the LISFLOOD model for Europe: current trends and way forward. Report for IES – JRC

Feyen, L. ,Vrugt, J. A. , Nuallin, B. , van der Knijff, J. M. and de Roo, A. P. J. (2007) Parameter optimisation and uncertainty assessment for large-scale streamflow simulation with the LISFLOOD model. *Journal of Hydrology*332 , pp. 276-289.

Feyen, L. ,Kalas, M. and Vrugt, J. (2008) Semi-distributed parameter optimization and uncertainty assessment for large-scale streamflow simulation using global optimization. *Hydrological Sciences Journal* 53 :(2) , pp. 293-308.

Gebremichael, M., & Hossain, F. (2010). Satellite rainfall applications for surface hydrology. Dordrecht: Springer.

Gellens-Meulenberghs, F.; Arboleda, A and Ghilain, N. , (2006) Status of development of the LSA-SAF evapotranspiration product. Proceedings of the 2nd LSA-SAF Training workshop, Lisbon, [8-10 March]

Gellens-Meulenberghs, F.; Arboleda, A and Ghilain, N. , (2007) Towards a continuous monitoring of evapotranspiration based on MSG data. Accepted contribution to the proceedings symposium on Remote sensing for environmental monitoring and change detection. IAHS series. IUGG, perugia , Italy

Haile, A. T., Rientjes, T., Gieske, A., & Gebremichael, M. (2010). Multispectral remote sensing for rainfall detection and estimation at the source of the Blue Nile River. *International Journal of Applied Earth Observation and Geoinformation, 12*(1), S76-S82.

Heinemann, T., A. Latanzo, et al. (2002). The Eumetsat multi-sensor precipitation estimate (MPE). Proceedings of the second International Precipitation Working Group, Madrid, Spain, IPWG.

Huffman, G.J., R.F. Adler, B. Rudolph, U. Schneider, and P. Keehn, 1995: Global Precipitation Estimates Based on a Technique for Combining Satellite-Based Estimates, Rain Gauge Analysis, and NWP Model Precipitation Information, *Journal of Climatology.*, 8, 1284-1295.

Huffman, G.J., 1997: Estimates of Root-Mean-Square Random Error for Finite Samples of Estimated Precipitation, J. Appl. Meteor., 1191-1201.

Huffman, G.J., R.F. Adler, P. Arkin, A. Chang, R. Ferraro, A. Gruber, J. Janowiak, A. McNab, B. Rudolph, and U. Schneider, 1997: The Global Precipitation Climatology Project (GPCP) Combined Precipitation Dataset, Bul. Amer. Meteor. Soc., 78, 5-20.

Huffman, G.J., R.F. Adler, D.T. Bolvin, G. Gu, E.J. Nelkin, K.P. Bowman, Y. Hong, E.F. Stocker, D.B. Wolff, 2007: The TRMM Multi-satellite Precipitation Analysis: Quasi-Global, Multi-Year, Combined-Sensor Precipitation Estimates at Fine Scale. J. Hydrometeor., 8(1), 38-55.

Huffman, G.J., R.F. Adler, M. Morrissey, D.T. Bolvin, S. Curtis, R. Joyce, B McGavock, J. Susskind, 2001: Global Precipitation at One-Degree Daily Resolution from Multi-Satellite Observations. J. Hydrometeor., 2(1), 36-50.

HYPRES (1996). "HYPRES database of hydraulic properties of European Soils." Retrieved 9 February 2011, from http://eusoils.jrc.ec.europa.eu/esdb_archive/ESDBv2/fr_advan.htm.

Iguchi, T., T. Kozu, et al. (2000)."Rain-Profiling Algorithm for the TRMM Precipitation Radar."*Journal of Applied Meteorology***39**(12): 2038-2052.

Inter Press Service, 2011 http://www.globalissues.org/news/2011/03/25/9041

J. G. Acker and G. Leptoukh, "Online Analysis Enhances Use of NASA Earth Science Data", Eos, Trans. AGU, Vol. 88, No. 2 (9 January 2007), pages 14 and 17.

Karssenberg, D., Wesseling, C. G., Burrough, P. A., & van Deursen, W. P. A. (1997). A simplified hydrological runoff model. Retrieved 16 August 2010, from http://pcraster.geo.uu.nl/models/catsop/index.html

Karssenberg, D. (2002) The value of environmental modelling languages for building distributed hydrological models.*Hydrological Processes 1*6 , pp. 2751-2766.

Karssenberg, D. (2002). "The value of environmental modelling languages for building distributed hydrological models." Hydrological Processes 16(14): 2751-2766.

Kinoti, J., Z. B. Su, et al. (2010). "Estimation of spatial-temporal rainfall distribution using remote sensing techniques: A case study of Makanya catchment, Tanzania." *International Journal of Applied Earth Observation and Geoinformation***12**(Supplement 1): S90-S99.

Kite, G.W., Ellehoj, E. and Dalton, A. 1996. 'GIS for Large-Scale Watershed Modelling'. In: Singh, V.P. and Fiorentino, M. (eds.) Geographical Information Systems in Hydrology. Kluwer. 443 p.

Kummerow, C., W. Barnes, et al. (2000). "The tropical rainfall measuring mission (TRMM) sensor package."*Journal of Atmospheric Oceanic Technology***15**(4): 809-817.

Lambe, T. W. and R. V. Whitman (1969).Description of an Assemblage of Particles, John Wiley & Sons.

Levizzani, V., Pinelli, F., Pasqui, M., Melani, S., Laing, A. G., & Carbone, R. E. (2010). A 10-year climatology of warm-season cloud patterns over Europe and the Mediterranean from Meteosat IR observations. [doi: DOI: 10.1016/j.atmosres.2010.05.014]. *Atmospheric Research, In Press, Corrected Proof.*

Lilly, A. (1997). A description of the HYPRES database (Hydraulic Properties of European Soils) . EC /JRC**:** 29-40.

LSA SAF (2010) The EUMETSAT Satellite Application Facility on Land Surface Analysis (LSA SAF) . Product uaser manual evapotranspiration (ET). http://landsaf.meteo.pt/algorithms.jsp?seltab=7&starttab=7#adescription

Masson, V.; Champeaux, J. L.; Chauvin, F.; Meriguet, C.; Lacaze, R. A. (2003). Global database of land surface parameters at 1km resolution in meteorological and climate models. Journal of Climate 16(9), 1261-1282

Michaelides, S., Levizzani, V., Anagnostou, E., Bauer, P., Kasparis, T., & Lane, J. E. (2009). Precipitation: Measurement, remote sensing, climatology and modeling. [doi: DOI: 10.1016/j.atmosres.2009.08.017]. *Atmospheric Research, 94*(4), 512-533.

Mulungu, D. M. M., & Munishi, S. E. (2007). Simiyu River catchment parameterization using SWAT model. [doi: DOI: 10.1016/j.pce.2007.07.053]. *Physics and Chemistry of the Earth, Parts A/B/C, 32*(15-18), 1032-1039.

Nash, J. E. and Sutcliffe, J. V. (1975) River flow forecasting through conceptual models, I: A discussion of principles. *Journal of Hydrology* 10 , pp. 282-290.

Ndomba, P., Mtalo, F., & Killingtveit, A. (2008). SWAT model application in a data scarce tropical complex catchment in Tanzania. [doi: DOI: 10.1016/j.pce.2008.06.013]. *Physics and Chemistry of the Earth, Parts A/B/C, 33*(8-13), 626-632.

NHS (2010, 17 August 2010). "Flood report archives." Retrieved 29 August 2010, from http://www.mawf.gov.na/index.html

Ranga, M.; Steven, W.; Running, J.; Glassy, P. (2000) User's Guide FPAR, LAI (ESDT: MOD15A2) 8-day Composite NASA MODIS Land Algorithm(Doc v1.0-09.14-jmg)

Rawls, W., D. Brakensiek, et al. (1982). "Estimation of Soil Water Properties."American Society of Agricultural Engineers 25.

Senthil-Kumar, S.; Luca, M.; Otto, S.; David, D. (2005) EUROPEAN DIGITAL ARCHIVE OF SOIL MAPS (EuDASM) SOIL MAPS OF AFRICA

Stisen, S., Jensen, K. H., Sandholt, I., & Grimes, D. I. F. (2008). A remote sensing driven distributed hydrological model of the Senegal River basin. [doi: DOI: 10.1016/j.jhydrol.2008.03.006]. *Journal of Hydrology, 354*(1-4), 131-148.

Theon, J. S. (1994). "The tropical rainfall measuring mission (TRMM)."Advances in Space Research**14**(3): 159-165.

TSDIS-P907 (2007). Vol. 4; Release 6.09. Retrieved January 2011, from http://pps.gsfc.nasa.gov/tsdis/Documents/ICSVol4.pdf.

UNESCO (1974). Soil Map of the World

USGS (2006).Shuttle Radar Topography Mission.College Park, Maryland, Global Land Cover Facility, University of Maryland.

van Biljon, S. (2007) Development of the SPLASH model: A deterministic conceptual daily rainfall-runoff model for southern Africa. SADC-HYCOS Phase 2 project report

van der Knijff, J. (2008). LISVAP Evaporation Pre-processor for the LISFLOOD Water Balance and Flood Simulation Model. Revised User Manual. Luxembourg, Joint Research Centre, European Commision. **ISSN 1018-5593:** 31.

van der Knijff, J. and A. De Roo (2008). LISFLOOD Distributed Water Balance and Flood Simulation Model. Revised User Manual. Luxembourg, Joint Research Centre, European Commision. **ISSN 1018-5593:** 109.

van der Knijff, J. M.; Younis, J. & De Roo, A. P. J., 2008, LISFLOOD: a GIS-based distributed model for river basin scale water balance and flood simulation, *International Journal of Geographical Information Science,*

Wesseling, C. G. , Karssenberg, D. , Burrough, P. A. and Van Deursen, W. P. A. (1996) Integrating dynamic environmental models in GIS: The development of a dynamic modelling language. Transactions in GIS 1, pp. 40-48.

Xie, P. and P. A. Arkin (1997)."A 17 year monthly analysis based on gauge observations, satellite estimates, and numerical model outputs."Bulletin of American Meteorological Society **78** (11): 2539-2558.

Zhao, R. J. and Liu, X. R. Singh, V. P. (ed) (1995) The Xinanjiang model. Computer Models of Watershed Hydrology pp. 215-232. Water Resources Publications, Highlands Ranch, CO

Websites:
http://www.meteona.com Namibia Meteorological Station (15 telemetry river flow stations in Cuvelai, and 20 telemetry rain gauges in Cuvelai, with NMS)
http://www.mawf.gov.na/Documents/april%20flood%20reports/09April10_17h00reading.pdf
http://www.weathersa.co.za/RSMC/login.jsp RSMC/SWFDP

http://wxmaps.org/pix/af.vv.html ECMW

http://earlywarning.usgs.gov/adds/imgbrowses2.php?image=dr&extent=af USGS or

http://edcftp.cr.usgs.gov/pub/edcuser/fewsips/africa/

http://rapidfire.sci.gsfc.nasa.gov/subsets/index2.php?project=FIRM&subset=Caprivi

http://envisat.esa.int/object/index.cfm?fobjectid=3772 ENVISAT ASAR

http://earth.esa.int/object/index.cfm?fobjectid=4001 ERS SAR

http://earth.esa.int/object/index.cfm?fobjectid=4070 ALOS PALSAR

In-text hyperlinks:

NASA – MIRADOR: http://disc.sci.gsfc.nasa.gov/additional/citing-our-data

http://mirador.gsfc.nasa.gov/cgi-bin/mirador/presentNavigation.pl?tree=project&project=TRMM&dataGroup=Gridded&dataset=3B42:%203-Hour%200.25%20x%200.25%20degree%20merged%20TRMM%20and%20other%20satellite%20estimates&version=006

http://www.eea.europa.eu/publications/COR0-landcover

ftp://ftp-fc.sc.egov.usda.gov/NSSC/Soil_Taxonomy/tax.pdf

http://eusoils.jrc.ec.europa.eu/esdb_archive/EuDASM/Africa/lists/ctz.htm

http://www.fao.org/wairdocs/ilri/x5546e/x5546e04.htm#

http://gdata1.sci.gsfc.nasa.gov/daac-bin/G3/gui.cgi?instance_id=TRMM_3B42_Daily.

http://geoserver.isciences.com:8080/geonetwork/srv/en/metadata.show?id=228

http://www.eea.europa.eu/publications/COR0-landcover

ftp://ftp-fc.sc.egov.usda.gov/NSSC/Soil_Taxonomy/tax.pdf

http://eusoils.jrc.ec.europa.eu/esdb_archive/EuDASM/africa/index.htm

http://www.fao.org/wairdocs/ilri/x5546e/x5546e04.htm#

http://pcraster.geo.uu.nl/documentation/pcrman/x181.htm#secdatbasemaptype

http://earthobservatory.nasa.gov/NaturalHazards/view.php?id=37730

http://www.limpoporak.com/en/river/geography/basins+of+southern+africa.aspx

http://earthobservatory.nasa.gov/NaturalHazards/view.php?id=37730

http://disc.sci.gsfc.nasa.gov/giovanni

http://gdata1.sci.gsfc.nasa.gov/daac-bin/G3/gui.cgi?instance_id=TRMM_3B42_Daily

https://lpdaac.usgs.gov/lpdaac/products/modis_products_table

http://www.ntsg.umt.edu/project/modis#data-product

http://postel.mediasfrance.org/en/BIOGEOPHYSICAL-PRODUCTS/Land-Cover/

http://www.lib.berkeley.edu/EART/fao.html

http://landsaf.meteo.pt.

http://www.ecmwf.int/research/EU_projects/GEOLAND/CTESSEL/index.html

ftp://e0srp01u.ecs.nasa.gov/srtm/version2/SRTM3/

http://www.unitar.org/unosat/node/44/1168

ftp://ftp-fc.sc.egov.usda.gov/NSSC/Soil_Taxonomy/tax.pdf

http://floods.jrc.ec.europa.eu/files/lisflood/ec_jrc_lisvapUserManual_JvdK.pdf

http://wxmaps.org/pix/soil10.html

http://www.cgiar-csi.org/data/elevation/item/45-srtm-90m-digital-elevation-database-v41

http://www.zki.dlr.de/map/214

http://www.unitar.org/unosat/node/44/1168

7. APPENDICES

7.1. Appendix 1TRMM V6 3B42 algorithm

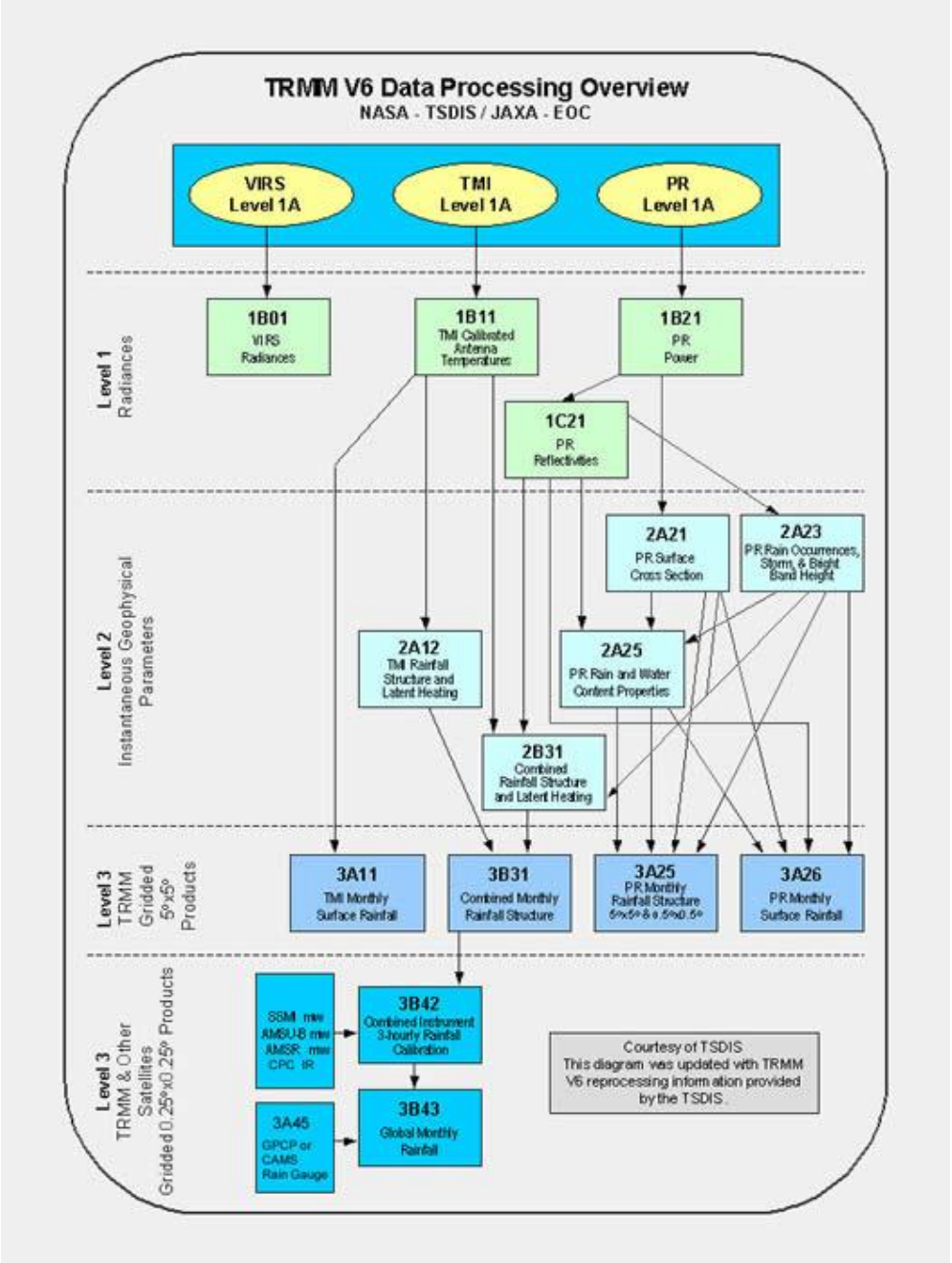

Source: Online Analysis Enhances Use of NASA Earth Science Data (*J. G. Acker and G. Leptoukh, 2007)*
http://disc.sci.gsfc.nasa.gov/precipitation/documentation/TRMM_README/TRMM_v6.shtml

7.2. Appendix 2Lisflood input maps[1]

Map	Name	Description
Mask	area.map	A boolean map that defines the model boundaries (values: true=1, false=0)
TOPOGRAPHY		
Local direction map	ldd.map	This file contains flow directions from each cell to its steepest neighbor (with value 1-9) 5 is a pit cell with no flow
Grad	gradient.map	Slope gradient [m m^{-1}]. Gradient equals tangent of slope in degrees]
Elevation range	elvrange.map	The difference between maximum and minimum elevation with a pixel [m]
LAND USE		
Land use	landuse.map	Map with CORINE land use classes
Forest	forest.map	Forest fraction for each cell. Values range from 0 (no forest at all) to 1 (pixel is 100% forest)
Direct runoff fraction	directrf.map	Fraction urban area for each cell. Values range from 0 (no urban area at all) to 1 (pixel is 100% urban)
SOIL		
Texture 1	soiltex1.map	Soil texture class layer 1 (Horizon A)
Texture 2	soiltex2.map	Soil texture class layer 2 (Horizon B)
Soil depth	soildep.map	Soil depth [cm] to bedrock or groundwater [cm]
CHANNEL GEOMETRY		
Channels	chan.map	Map with Boolean 1 for all channel pixels, and Boolean 0 for all other pixels on mask map
Channel gradient	changrad.map	Channel gradient [m m^{-1}]
Channel Manning	chanman.map	Manning's roughness coefficient for channels
Channel length	chanleng.map	Channel length [m]
Channel bottom width	chanbw.map	Channel bottom width [m]
Chan SdXdY	chans.map	Channel side slope [mm^{-1}]. It is defined as horizontal distance divided by vertical distance (dx/dy), whilst normally slope is expected to be defined as (dy/dx)
ChanDepth Threshold	Chanbnkf.map	Bankful channel depth [m]
METEOROLOGICAL VARIABLES		
Map	**Prefix**	**Description**
Precipitation	pr	Precipitation rate [mm day^{-1}]
Tavg	ta	Average daily temperature [°C]
EO	e	Daily potential evaporation rate free water surface [mm day^{-1}]
ESO	es	Daily potential evaporation rate, bare soil [mm day^{-1}]
ETO	et	Daily potential evapotranspiration rate reference crop [mm day^{-1}]
DEVELOPMENT OF VEGETATION OVER TIME		
Map	**Prefix**	**Description**
LAI	lai	Pixel-average Leaf Area Index [m^2 m^{-2}]
DEFINITION OF INPUT/OUTPUT TIMESERIES		
Map	**Name**	**Description**
Gauges	outlets.map	Locations at which discharge timeseries are reported [nominal map]
Sites	sites.map	Locations at which timeseries of intermediate state and rate variables are reported [nominal map]

[1]Source distributed water balance and flood simulation model, revised user manual [*Van der Knijff and De Roo, 2008*]

7.3. Appendix 3 List of PCRaster codes used for the study

asc2map *--clone*clone.*map*-*B -a* clone.*txt*area.*map*
asc2map *--clone* area.*map* *-S -a* dem.*txt*dem.*map*
asc2map *--clone* area.*map* *-B -a* chan.*txt* chan.*map*
asc2map *--clone* area.*map* *-O -a* soils.*txt* soiltex1.*map*
asc2map *--clone* area.*map* *-N–a* soildepth.*txt* soildep.*map*
asc2map *--clone* area.*map* *-S –a* forest.*txt* forest.*map*
asc2map *--clone* area.*map* *-D–a* landuse.*txt* landuse.*map*
asc2map *--clone* area.*map* *-S -a* channelgradient.*txt* changrad.*map*
asc2map *--clone* area.*map* *-S –a* channel_length.*txt* chanleng.*map*
asc2map *--clone* area.*map* *-S –a* chan_sideslope.*txt* chans.*map*
asc2map *--clone* area.*map* *-S -a* channels.*txt* chan.*map*
asc2map *--clone* area.*map* *-S -a* chan_mannings.*txt* chanman.*map*
asc2map *--clone* area.*map* *-S -a* chanbottomwidth.*txt* chanbw.*map*
asc2map *--clone* area.*map* *-S -a* chanbankfulldepth.*txt* chanbnkf.*map*
asc2map *--clone* area.*map* *-S –a* elevation_range.*txt* elvrange.*map*
asc2map *--clone* area.*map* *-S –a* gradient.*txt* gradient.*map*
asc2map *--clone* area.*map* *-S –a* pr001.*txt* pr000000.001.*map* (rainfall maps from 1 to 1+…. timestep)
asc2map *--clone* area.*map* *-S -a* lai001.*txt* lai00000.000.*map*
asc2map *--clone* area.*map* *-S –a* e001.*txt* e0000000.001.*map*
asc2map *--clone* area.*map* *-S –a* et0001.*txt* et000000.001.*map*
asc2map *--clone* area.*map* *-S –a* es0001.*txt* es0000000.001.*map* (soil evaporation maps)
asc2map *--clone* area.*map* *-N –a* sites.*txt*sites.*map*
asc2map *--clone* area.*map* *-N -a* gauges.*txt*outlets.*map*
pcrcalc ldd.*map* = *lddcreate* (dem.*map*, 1E35, 1E35, 1E35, 1E35)
pcrcalc *--lddin* lddedited.*map* = lddcreate(dem.*map*,1E35,1E35,1E35,1E35) (cleans up pits on edges of ldd)

7.4. Appendix 4 Lisflood parameter derivation equations[2]

	Parameter	Equation
Int	Interception	$Int = Smax \times [1 - \exp(-k \times R\Delta t/Smax)]$
		$Smax$ is calculated using an empirical equation
		R is the dailyrainfallintensity in millimeters.
		k a factor to account for the density of the vegetation.
		Δt is a change in timestep.
EW_{int}	Evaporationfrom the interception store	$EW_{int} = \min(EW_{max} \times \Delta t, Int_{cum})$
		Int_{cum} is the average water in the interception store in mm.
		EW_{max} is the maximum evaporation per timestep
D_{int}	Leaf drainage per time step	$D_{int} = 1/T_{int} \times Int_{cum}\Delta t$
		T_{int} is a time constant for the store in days, which is set to 1 day.
		Int_{cum} is the average water in the interception store.
ES_a	Actualsoilevaporation	$ES_a = \min(ES_{a,}w_1 - w_{res1})$
		w_1 the amount of moisture [mm] in the uppersoillayer
		w_{res1} the amount [mm] of residualsoilmoisture
T_a	Actualtranspiration	$T_a = r_{ws} \times T_{max}$
		r_{ws} reduction factor to simulate low soil moisture content
		T_{max} maximum transpiration per timestep [mm]
INF_{act}	Infiltration	$INF_{act} = \min(INF_{pot,}W_{av} - D_{pref,gw})$
		$INF_{pot,}$ infiltration capacity [mm]
		W_{av} amount of water available for infiltration
		$D_{pref,gw}$ amount of preferential flow per timestep [mm]
R_s	Surfacerunoff	$R_s = R_d + (1 - f_{dr}) \times (W_{av} - D_{pref,gw} - INF_{act}$
$D_{1,2}$	Drainage from top to subsoil	$D_{1,2} = \min[K_1(w_1')\Delta t, w_{s2}' - w_2']$
		$K_1(w_1')$soil water conductivity
		$w_{s2}' - w_2'$ change in amount of soil moisture [mm]
$D_{2,gw}$	Drainage from subsoil to upper ground water	$D_{2,gw} = \min[K_2(w_2')\Delta t, w_2' - w_{r2}']$
		w_{r2}' residual soil moisture [mm]
$D_{pref,gw}$	Amount of preferential flow per timestep	$D_{pref,gw} = w_{av}(w_1/w_{s1})^{cpref}$
		w_1 total moisture storage in the upper soil layer [mm]
		w_{s1} maximum storage of soil moisture in the upper layer [mm]
$D_{uz,lz}$	Drainage from upper to lower ground zone	$D_{uz,lz} = \min(\mathrm{GW_{perc}} \times \Delta\mathrm{t}, \mathrm{UZ})$
		$\mathrm{GW_{perc}}$ calibration constant [mm/day]
		UZ water stored in the upper zone
Q_{lz}	Outflow from lower groundwater zone	$Q_{lz} = 1/T_{lz} \times LZ\Delta t$
		T_{lz} a reservoir constant in days
		LZ amount of water stored in the lower zone [mm]
Q_{uz}	Outflow from upper groundwater zone	$Q_{uz} = 1/T_{uz} \times UZ\Delta t$
		T_{uz} amount of water stored in the upper zone [mm]
D_{loss}	Loss from lower groundwater zone	$D_{loss} = f_{loss} \times Q_{lz}$
		f_{loss} loss fraction

[2] Source: LISFLOOD revised user manual (*van der Knijff and de Roo 2008*)

7.5. Appendix 5 CORINE landuse nomenclature

Level 1	Level 2	Level 3
1. Artificial surfaces	1.1. Urban fabric	1.1.1. Continuous urban fabric
		1.1.2. Discontinuous urban fabric
	1.2. Industrial, commercial and transport units	1.2.1. Industrial or commercial units
		1.2.2. Road and rail networks and associated land
		1.2.3. Port areas
		1.2.4. Airports
	1.3. Mine, dump and construction sites	1.3.1. Mineral extraction sites
		1.3.2. Dump sites
		1.3.3. Construction sites
	1.4. Artificial non-agricultural vegetated areas	1.4.1. Green urban areas
		1.4.2. Sport and leisure facilities
2. Agricultural areas	2.1.Arable land	2.1.1. Non-irrigated arable land
		2.1.2. Permanently irrigated land
		2.1.3. Rice fields
	2.2. Permanent crops	2.2.1. Vineyards
		2.2.2. Fruit trees and berry plantations
		2.2.3. Olive groves
	2.3. Pastures	2.3.1. Pastures
	2.4. Heterogeneous agricultural areas	2.4.1. Annual crops associated with permanent crops
		2.4.2. Complex cultivation
		2.4.3. Land principally occupied by agriculture, with significant areas of natural vegetation
		2.4.4. Agro-forestry areas
3. Forests and semi-natural areas	3.1. Forests	3.1.1. Broad-leaved forest
		3.1.2. Coniferous forest
		3.1.3. Mixed forest
	3.2. Shrub and/or herbaceous	3.2.1. Natural grassland vegetation association
		3.2.2. Moors and heathland
		3.2.3. Sclerophyllous vegetation
		3.2.4. Transitional woodland shrub
	3.3. Open spaces with little	3.3.1. Beaches, dunes, and sand plains or no vegetation
		3.3.2. Bare rock
		3.3.3. Sparsely vegetated areas
		3.3.4. Burnt areas
		3.3.5. Glaciers and perpetual snow
4. Wetlands	4.1. Inland wetlands	4.1.1. Inland marshes
		4.1.2. Peatbogs
	4.2. Coastal wetlands	4.2.1. Salt marshes
		4.2.2. Salines
		4.2.3. Intertidal flats

Source: http://www.ceh.ac.uk/data/LCM1990Categories.html

7.6. Appendix 6 LSA SAF ET algorithm

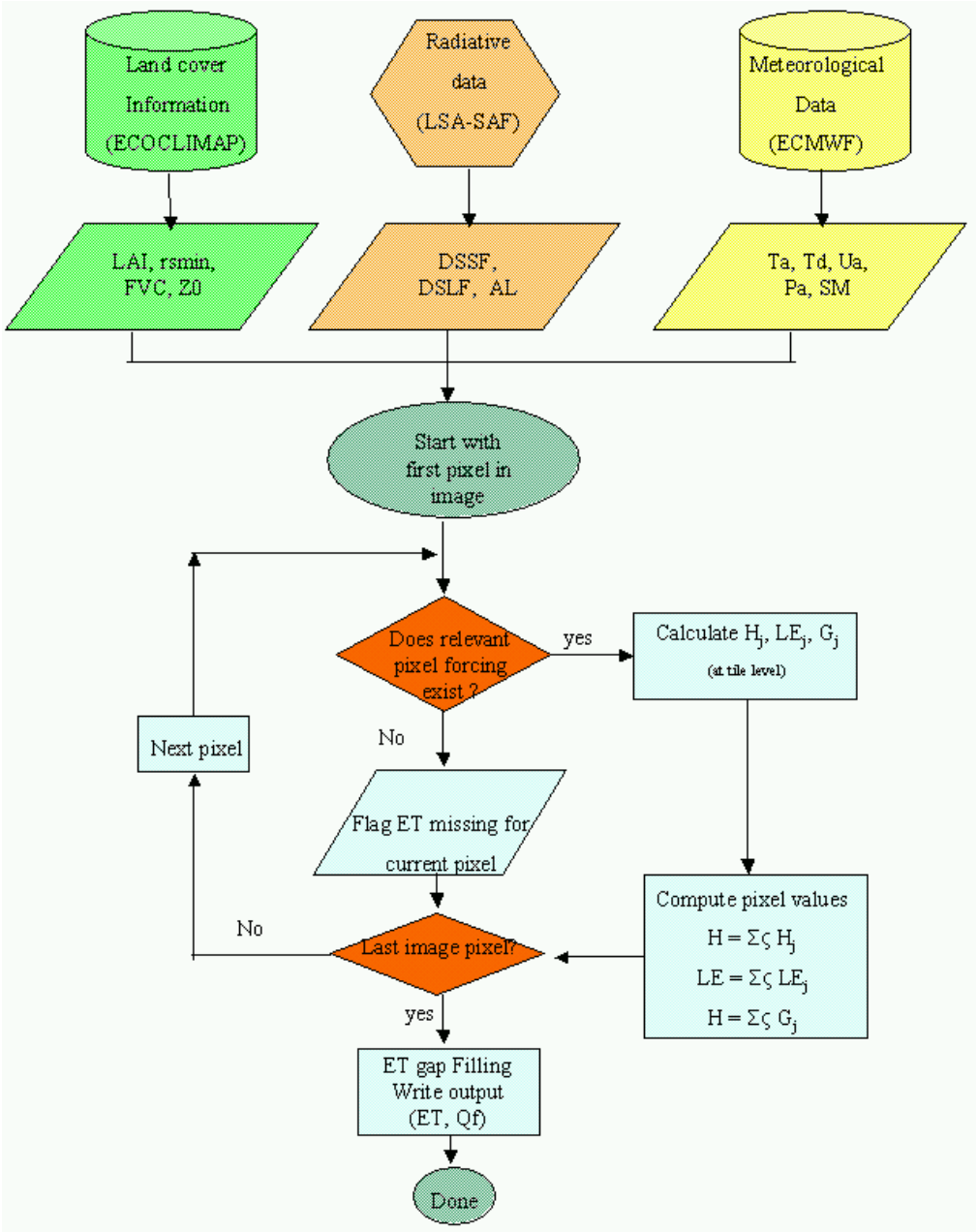

Source: http://landsaf.meteo.pt/algorithms.jsp?seltab=7&starttab=7#adescription